

Aging Wiener-Khinchin theorem and critical exponents of $1/f^\beta$ noise

N. Leibovich,¹ A. Dechant,^{1,2} E. Lutz,² and E. Barkai¹

¹*Department of Physics, Institute of Nanotechnology and Advanced Materials, Bar Ilan University, Ramat-Gan 52900, Israel*

²*Department of Physics, Friedrich-Alexander-Universität Erlangen-Nürnberg, 91058 Erlangen, Germany*

(Received 20 March 2016; revised manuscript received 7 August 2016; published 17 November 2016)

The power spectrum of a stationary process may be calculated in terms of the autocorrelation function using the Wiener-Khinchin theorem. We here generalize the Wiener-Khinchin theorem for nonstationary processes and introduce a time-dependent power spectrum $\langle S_m(\omega) \rangle$ where t_m is the measurement time. For processes with an aging autocorrelation function of the form $\langle I(t)I(t+\tau) \rangle = t^\chi \phi_{\text{EA}}(\tau/t)$, where $\phi_{\text{EA}}(x)$ is a nonanalytic function when x is small, we find aging $1/f^\beta$ noise. Aging $1/f^\beta$ noise is characterized by five critical exponents. We derive the relations between the scaled autocorrelation function and these exponents. We show that our definition of the time-dependent spectrum retains its interpretation as a density of Fourier modes and discuss the relation to the apparent infrared divergence of $1/f^\beta$ noise. We illustrate our results for blinking-quantum-dot models, single-file diffusion, and Brownian motion in a logarithmic potential.

DOI: [10.1103/PhysRevE.94.052130](https://doi.org/10.1103/PhysRevE.94.052130)

I. INTRODUCTION

In many applications, a random process $I(t)$ recorded in a time interval $[0, t_m]$ is analyzed using the sample spectrum $S_m(\omega) = |\int_0^{t_m} I(t') \exp(-i\omega t') dt'|^2 / t_m$, where the measurement time t_m is assumed to be long. For a stationary process, the power spectrum is routinely calculated from the autocorrelation function $C(\tau) = \langle I(t)I(t+\tau) \rangle$, using the Wiener-Khinchin theorem [1,2]

$$\lim_{t_m \rightarrow \infty} \langle S_m(\omega) \rangle = 2 \int_0^\infty d\tau C(\tau) \cos(\omega\tau). \quad (1)$$

Obviously, not all physical processes are stationary [3–15] and then the Wiener-Khinchin theorem (1) does not hold. Extending the Wiener-Khinchin theorem to nonstationary processes has been a topic of many works [16–19]. Some relate it to the instantaneous power spectrum, where it loses its meaning as a density since it may get negative values (e.g., [16,17]). Others deal with a specific process such as telegraphic noise [18] or periodically driven stochastic systems [19].

We here consider the power spectrum of systems exhibiting scale invariant aging with an autocorrelation function of the form $C(t, \tau) \sim t^\chi \phi_{\text{EA}}(\tau/t)$, where $(\dots)_{\text{EA}}$ refers to the ensemble average. Such autocorrelation functions appear in a vast array of systems and models ranging from glassy dynamics [10,20,21], blinking quantum dots [22], laser-cooled atoms [23,24], motion of a tracer particle in a crowded environment [25,26], elastic models of fluctuating interfaces [27], diffusion in heterogeneous environment [28], deterministic noisy Kuramoto models [29], granular gases [30], deterministic intermittency [31], to growing interfaces following the Kardar-Parisi-Zhang (KPZ) equation [32,33]. In our recent publications [34,35], we have generalized the Wiener-Khinchin theorem to these aging processes by introducing a time-dependent spectral density. We have moreover established a correspondence to $1/f^\beta$ noise when $\phi_{\text{EA}}(x)$ is not analytic for small arguments.

The power spectrum of $1/f^\beta$ noise (sometimes simply called $1/f$ noise) at low frequencies is

$$S(\omega) \sim \omega^{-\beta}, \quad 0 < \beta < 2. \quad (2)$$

The value $\beta = 0$ corresponds to white noise and $\beta = 2$ to Brownian noise. $1/f^\beta$ noise, with a range of different exponents, occurs in many systems in a variety of disciplines. A partial list includes electronic, solid and condensed matter devices [36–39], sand-pile models [40], blinking quantum dots [41,42], nanoscale electrodes [43], geophysics including weather data [44,45], experimental data of voltage-dependent anion channel in rats' brains [46], and processes modeled by nonlinear-stochastic-differential equations [47].

In [48], Mandelbrot suggested that “one needs a non-Wienerian spectral theory to account for $f^{\theta-2}$ noise,” where a spectrum dependent on the length of the time series might be measured [48,49]. Indeed, as shown theoretically [5,6,50] and experimentally [43,51], the power spectrum of a blinking quantum dot and of nanoelectrodes ages, namely, as the measurement time becomes longer the intensity of the measured noise is reduced, decaying as a power law.

Traditional studies of $1/f^\beta$ noise characterize the spectrum with a single exponent β . In the recent experiment of Ref. [51], the aging properties of $1/f^\beta$ noise were characterized with the help of five different exponents β , z , μ , η , and δ defined as follows: the asymptotic power spectrum is of the form $S(\omega) \sim A_{t_m} \omega^{-\beta}$ with the time-dependent amplitude $A_{t_m} \sim (t_m)^{-z}$ for long times and low-frequency cutoff $\omega_{\text{min}} \sim (t_m)^{-\eta}$. Furthermore, the “power” at zero frequency is $S(0) \sim (t_m)^\mu$ and the total measured power $\int_{1/t_m}^\infty S(\omega) d\omega \sim (t_m)^\delta$. Our aim here is to derive these five exponents from the scale invariant autocorrelation function for aging processes and investigate their relationships. We apply our finding to blinking-quantum-dot models [22], as well as to single-file diffusion [25,26] and diffusion in a logarithmic potential [23,24]. Sample paths of these models, i.e., a representative time trace of these processes, are shown in Fig. 1. Visually these processes appear very different; the underlying unifying theme is their description in terms of a scale invariant autocorrelation function which leads to $1/f^\beta$ noise.

For stationary processes, the spectrum is related to the discrete Fourier modes at the natural frequencies $\omega_n = 2\pi n/t_m$ with n integer [1]. The integral of the spectrum over all frequencies is finite and equal to the sum of the Fourier

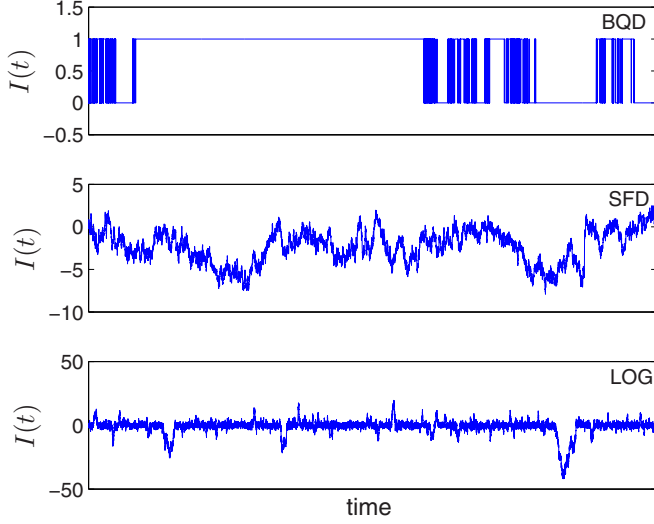


FIG. 1. Time traces of the three models: blinking-quantum-dot (BQD) model with $\alpha = 0.8$ (upper panel), single-file diffusion (SFD) with $D = 0.5$ and $a = 1$ (middle panel), and Brownian motion in a logarithmic potential (lower panel). See details on each model in Secs. VII, VIII, and IX (respectively).

modes' intensities. Since the spectrum is thus positive and normalizable, we can interpret it as the continuous distribution of Fourier modes in the limit of infinite measurement time. By contrast, $1/f^\beta$ noise with $\beta > 1$ exhibits a nonintegrable infrared divergence and thus infinite power, which has led to some discussions on its physical interpretation [5,48,49]. We comment that in some (although not many) systems, regardless of stationarity, a low-frequency cutoff can be found at low frequencies. This cutoff may render the power spectrum integrable (see [36,38,52] and the references therein). For other systems, no cutoff has ever been observed. Here, we show that allowing a measurement-time-dependent spectrum naturally resolves this apparent convergence paradox, as the power remains finite at finite times. Thus, even for nonstationary processes, the spectrum retains its interpretation as a density in frequency space. While for finite measurement times the detectable Fourier modes are of course discrete, we argue that, nevertheless, the spectrum can also be understood as a continuous function of frequency. This function then exhibits scale invariant oscillations, which can yield additional information on the critical exponents not contained in the natural frequencies.

The outline of the paper is the following. In Secs. II and III, we derive the generalized Wiener-Khinchin theorem connecting the aging autocorrelation function $C(t, \tau)$ and the time-dependent spectral density $S_{t_m}(\omega)$. In Sec. IV, we evaluate explicitly the spectral density for a scale invariant autocorrelation function and discuss the relationship with $1/f^\beta$ noise. We then compute in Sec. V the five critical exponents characterizing $1/f^\beta$ noise. In Sec. VI, we compare the properties of the time-dependent spectrum to the stationary case and discuss its relation to Fourier modes. Finally, in Secs. VII, VIII, and IX, we apply our results to concrete examples: blinking quantum dot, single-file diffusion, and diffusion in a logarithmic potential, respectively.

II. AGING POWER SPECTRUM: THE TIME-AVERAGED FORMALISM

For a nonstationary process, the ensemble-averaged autocorrelation function is $\langle I(t)I(t + \tau) \rangle = C(t, \tau)$ and depends explicitly on the time t and the lag time τ . To examine analytically the temporal behavior of the power spectrum, we follow Mandelbrot [48] and define the power spectrum of a random signal $I(t)$ as $S_{t_m}(\omega) = |\hat{I}_{t_m}(\omega)|^2/t_m$ where $\hat{I}_{t_m}(\omega) = \int_0^{t_m} I(t') \exp(-i\omega t') dt'$, and t_m is the measurement time. The spectrum, by this definition, is

$$\langle S_{t_m}(\omega) \rangle = \left\langle \frac{1}{t_m} \int_0^{t_m} dt_1 I(t_1) e^{-i\omega t_1} \int_0^{t_m} dt_2 I(t_2) e^{+i\omega t_2} \right\rangle. \quad (3)$$

Equivalently, we can write

$$\begin{aligned} \langle S_{t_m}(\omega) \rangle &= \frac{1}{t_m} \int_0^{t_m} dt_1 \int_{t_1}^{t_m} dt_2 \langle I(t_1)I(t_2) \rangle e^{-i\omega(t_1-t_2)} \\ &+ \frac{1}{t_m} \int_0^{t_m} dt_1 \int_0^{t_1} dt_2 \langle I(t_1)I(t_2) \rangle e^{-i\omega(t_1-t_2)}, \end{aligned} \quad (4)$$

where the first term on the right side corresponds to $t_1 < t_2$, and the second term is for $t_2 < t_1$. In order to express Eq. (4) in terms of the autocorrelation function we first change the integration order and the names of integration variables ($t_1 \leftrightarrow t_2$) to find

$$\begin{aligned} \langle S_{t_m}(\omega) \rangle &= \frac{1}{t_m} \int_0^{t_m} dt_1 \int_{t_1}^{t_m} dt_2 \langle I(t_1)I(t_2) \rangle \\ &\times [e^{i\omega(t_1-t_2)} + e^{-i\omega(t_1-t_2)}]. \end{aligned} \quad (5)$$

An additional change of variables $t_1 = t_1$ and $t_2 - t_1 = \tau$ gives

$$\langle S_{t_m}(\omega) \rangle = \frac{2}{t_m} \int_0^{t_m} dt_1 \int_0^{t_m-t_1} d\tau \langle I(t_1)I(t_1 + \tau) \rangle \cos(\omega\tau). \quad (6)$$

By interchanging the order of integration, we finally obtain [50]

$$\langle S_{t_m}(\omega) \rangle = \frac{2}{t_m} \int_0^{t_m} d\tau (t_m - \tau) \langle C_{TA}(t_m, \tau) \rangle \cos(\omega\tau), \quad (7)$$

where the time-averaged autocorrelation function is defined as

$$C_{TA}(t_m, \tau) = \frac{1}{t_m - \tau} \int_0^{t_m-\tau} dt_1 I(t_1)I(t_1 + \tau). \quad (8)$$

We emphasize that the ensemble- and time-averaged autocorrelation functions $C(t, \tau)$ and $C_{TA}(t_m, \tau)$ are not identical for the underlying processes considered in this paper. In the following, we consider time-averaged autocorrelation functions of the scaling form

$$\langle C_{TA}(t_m, \tau) \rangle = t_m^\gamma \varphi_{TA}(\tau/t_m). \quad (9)$$

For the time being, we assume that this asymptotic scaling is valid for all τ and t_m . For real physical systems this is an approximation, as we discuss in Secs. VII–IX. We also assume that $\langle I \rangle$ is a constant independent of time (see further discussion in Appendix A). Substituting Eq. (9) in Eq. (7) and changing variables ($x = \tau/t_1$), we obtain what we call the time-averaged form of the aging Wiener-Khinchin theorem

$$\langle S_{t_m}(\omega) \rangle = 2t_m^{\gamma+1} \int_0^1 dx (1-x) \varphi_{TA}(x) \cos(\omega t_m x). \quad (10)$$

By using a cosine transform [53] we further find

$$t_m^\Upsilon \varphi_{\text{TA}}(x) = \frac{1}{2\pi(1-x)} \int_{-\infty}^{\infty} d\omega \langle S_{t_m}(\omega) \rangle \cos(\omega t_m x), \quad (11)$$

where $0 < x < 1$ and $\langle S_{t_m}(\omega) \rangle$ is an even function. Equation (11) establishes a direct connection between the scaling function $\varphi_{\text{TA}}(x)$ and the average power spectrum $\langle S_{t_m}(\omega) \rangle$. Care must be taken when evaluating information on the underlying autocorrelation function from the sample spectrum (see discussion in Appendix B).

Note that the spectrum ages, i.e., it depends on the measurement time t_m (when the measurement started at $t = 0$), namely, as the measurement time becomes longer the intensity of the measured noise might change, reflecting the aging of the system.

III. AGING POWER SPECTRUM: THE ENSEMBLE-AVERAGED FORMALISM

In this section, we derive a relation between the ensemble-averaged autocorrelation function $C(t, \tau)$ and the average time-dependent power spectrum $\langle S_{t_m}(\omega) \rangle$. We assume, as before, that the autocorrelation function scales as

$$C(t, \tau) = t^\Upsilon \phi_{\text{EA}}(\tau/t) \quad (12)$$

at all times τ and t . Systems which exhibit this type of correlation scaling behavior have been discussed in Refs. [10,20–22,25–27,29–31,33,54]. By taking the ensemble average of Eq. (8), we directly obtain a connection between time and ensemble-averaged correlation functions

$$\varphi_{\text{TA}}(x) = \frac{x^{\Upsilon+1}}{1-x} \int_{\frac{x}{1-x}}^{\infty} dy \frac{\phi_{\text{EA}}(y)}{y^{2+\Upsilon}}. \quad (13)$$

Let us first assume $\Upsilon = 0$. Then, substituting Eq. (13) in Eq. (10) and changing the integration order we find

$$\langle S_{t_m}(\omega) \rangle = 2t_m \int_0^{\infty} dx \phi_{\text{EA}}(x) \int_0^{1/(1+x)} d\tilde{t}_1 \cos(\tilde{\omega}\tilde{t}_1 x) \tilde{t}_1. \quad (14)$$

Integrating by parts gives

$$\langle S_{t_m}(\omega) \rangle = 2t_m \int_0^{\infty} dx \phi_{\text{EA}}(x) \times \left[\frac{\sin(\tilde{\omega}\frac{x}{1+x})}{\tilde{\omega}x(1+x)} + \frac{\cos(\tilde{\omega}\frac{x}{1+x})}{\tilde{\omega}^2 x^2} - \frac{1}{\tilde{\omega}^2 x^2} \right]. \quad (15)$$

Again changing variables according to $y = x/(1+x)$ eventually gives

$$\langle S_{t_m}(\omega) \rangle = 2t_m \int_0^1 \frac{dy}{(\tilde{\omega}y)^2} \phi_{\text{EA}}\left(\frac{y}{1-y}\right) \times [\tilde{\omega}y \sin(\tilde{\omega}y) + \cos(\tilde{\omega}y) - 1], \quad (16)$$

where $\tilde{\omega} = \omega t_m$.

For $\Upsilon \neq 0$, we find in a similar manner

$$\langle S_{t_m}(\omega) \rangle = 2t_m \int_0^{\infty} dx \phi_{\text{EA}}(x) \int_0^{1/(1+x)} d\tilde{t}_1 \cos(\tilde{\omega}\tilde{t}_1 x) \tilde{t}_1^{\Upsilon+1}. \quad (17)$$

Evaluating the last integral explicitly [55], we finally arrive at

$$\langle S_{t_m}(\omega) \rangle = \frac{2t_m^{\Upsilon+1}}{2+\Upsilon} \int_0^1 dy (1-y)^\Upsilon \phi_{\text{EA}}\left(\frac{y}{1-y}\right) \times {}_1F_2\left[1 + \frac{\Upsilon}{2}; \frac{1}{2}, 2 + \frac{\Upsilon}{2}; -\left(\frac{\tilde{\omega}y}{2}\right)^2\right], \quad (18)$$

where ${}_1F_2[a; b_1, b_2; z]$ refers to the hypergeometric function and $\Upsilon > -2$ for convergence. Equation (18) is our second aging Wiener-Khinchin theorem connecting the ensemble-averaged scaling autocorrelation function ϕ_{EA} to the sample spectrum. The inverse formula, which relates the power spectrum to the ensemble-averaged autocorrelation function is

$$C(t_m - \tau, \tau) = \frac{1}{\pi} \int_0^{\infty} d\omega \cos(\omega\tau) \left[\langle S_{t_m}(\omega) \rangle + t_m \frac{\partial}{\partial t_m} \langle S_{t_m}(\omega) \rangle \right]. \quad (19)$$

This inversion is general and valid for any type of autocorrelation function.

Equations (10) and (18) provide two forms of the aging Wiener-Khinchin theorem, relating the sample spectrum to either the time- or ensemble-averaged scaling autocorrelation function. The choice between the theorems depends on the practical application. Most theoretical works provide an ensemble-averaged autocorrelation function $\phi_{\text{EA}}(x)$. In this case, to use Eq. (10) we need to determine the time-averaged autocorrelation function from Eq. (13) first. On the other hand, to use Eq. (18) we need to determine the time dependency of the autocorrelation function, in particular the exponent Υ , which in experimental situations is *a priori* unknown, although it could be estimated from data. In addition, the inverse formula (19) contains a derivative term, which may increase measurement errors (see Appendix B where the inversion is performed for a specific example). Still, both formalisms are clearly equivalent and useful.

IV. SCALE INVARIANT AUTOCORRELATION FUNCTION AND THE POWER SPECTRUM

Our goal now is to relate explicitly the spectral density for the scale invariant autocorrelation function and discuss the relationship with $1/f^\beta$ noise. We assume an additional characteristic behavior of the scaling function; the autocorrelation function $\phi_{\text{EA}}(x)$ is asymptotically of the polynomial form

$$\phi_{\text{EA}}(x) \approx \begin{cases} a_0 - a_V x^V + \dots, & x \ll 1 \\ b_0 - b_\Lambda x^\Lambda + \dots, & x \gg 1 \end{cases} \quad (20)$$

where a_0, b_0, a_V , and b_Λ are constants which are determined by the specific process. Processes that possess such a behavior are given in Refs. [21–23,25–30,33,37] (see also Table I). Using Eq. (13) we find the time-averaged autocorrelation function

$$\varphi_{\text{TA}}(x) \approx \begin{cases} \tilde{a}_0 - \tilde{a}_V x^V + \tilde{a}_1 x + \dots, & x \ll 1 \\ \tilde{b}_0 (1-x)^\Upsilon - \tilde{b}_\Lambda (1-x)^{\Upsilon-\Lambda} + \dots, & 1-x \ll 1 \end{cases} \quad (21)$$

where $\tilde{a}_0 = a_0/(1+\Upsilon)$, $\tilde{b}_0 = b_0/(1+\Upsilon)$, $\tilde{a}_V = a_V/(1+\Upsilon-V)$, and $\tilde{b}_\Lambda = b_\Lambda/(1+\Upsilon-\Lambda)$. We assume $0 < |V| < 1$,

TABLE I. The aging behavior of several models, where the autocorrelation function is given in terms of $\langle I(t)I(t+\tau) \rangle \sim t^\Upsilon \phi_{\text{EA}}(\tau/t)$ and $\phi_{\text{EA}}(x) \propto a_0 - a_V x^V$ when $x \ll 1$.

Model [Ref.]	Exponent range	Υ	V	Method
Unilayer Parisi's tree [21]	$0 < \alpha < 1$	0	$\alpha - 1$	Analytic
Blinking quantum dot [22]	$0 < \alpha < 1$	$0^a, 2\alpha - 2^b$	$\alpha - 1^a, 1 - \alpha^b$	Analytic
Laser-cooled atoms [23]	$1 < \alpha < 3$	$2 - \alpha$	$2 - \alpha$	Analytic
Single-file diffusion [25,26]		1/2	1/2	Analytic
Generalized elastic model [27]	$0 < \alpha < 1$	α	α	Analytic
Coupled classical oscillators ^c [29]		$[-0.02, 0]^d [-0.58, -0.4]^e$	$-0.14 \pm 0.03^d 0^e$	Numeric
(1+1)D KPZ class [32]		2/3	2/3	Analytic
(1+1)D KPZ interfaces in LC turbulence [33,57]		$\approx 0.66^f$	≈ 0.66	Experiment
(2+1)D DP class [58]		≈ 0.901		Numeric
(2+1)D DP transition in LC turbulence [59]		≈ 0.9		Experiment
Infinite RC transmission line [37]	$1 < \alpha < 2$	$\alpha - 1$	$\alpha - 1$	Analytic
2D Glauber-Ising model [60,61]		$\approx 0.115^g$		Numeric
		0^h		Analytic

^aPower-law "on"/"off" waiting time [22].

^bFinite mean "on" time [22].

^cLattice size 32×32 , coupling strength $\kappa = -4$ [29].

^dIntermediate regime (ii) (see details in [29]).

^eSaturation regime (iii) (see details in [29]).

^fThe exponent $\Upsilon = 2\beta$ where β was measured as ≈ 0.33 .

^gQuench from disordered configuration to critical temperature.

^hQuench from disordered configuration to low temperature.

$\Upsilon - V > -1$, $\Lambda < 0$, and $\Upsilon - \Lambda > -1$ for convergence. These conditions are naturally satisfied for all relevant examples (see Table I and Secs. VII–IX).

Using Eq. (10), the power spectrum for such a process in the limit $\omega t_m = 2\pi n$, where n is a large positive integer, is

$$\langle S_{t_m}(\omega) \rangle_{\omega t_m = 2\pi n} \approx 2\tilde{a}_V \frac{\sin(\pi V/2)\Gamma(1+V)}{t_m^{-\Upsilon+V} \omega^{1+V}}. \quad (22)$$

Accordingly, the scale invariant autocorrelation function (20) leads to $1/f^\beta$ noise. The next leading terms are

$$\begin{aligned} \langle S_{t_m}(\omega) \rangle_{\omega t_m \gg 1} &\approx 2\tilde{a}_V \frac{\sin(\pi V/2)\Gamma(1+V)}{t_m^{-\Upsilon+V} \omega^{1+V}} \\ &+ \frac{2(a_0 - \tilde{a}_1)}{\omega^2 t_m^{-\Upsilon+1}} - 2\tilde{b}_0 \frac{\Gamma(2+\Upsilon) \cos(\omega t_m - \Upsilon\pi/2)}{\omega^{2+\Upsilon} t_m} \\ &+ 2\tilde{b}_\Lambda \frac{\Gamma(2+\Upsilon-\Lambda) \cos[\omega t_m - (\Upsilon-\Lambda)\pi/2]}{\omega^{2+\Upsilon-\Lambda} t_m^{-\Lambda+1}} \end{aligned} \quad (23)$$

(see derivation in [35]). When ωt_m is treated as a continuous variable, Eq. (23) exhibits oscillations. For specific examples, these oscillations are discussed in Secs. VII–IX. The conditions on the exponents Υ , V , and Λ guarantee that the $1/f^\beta$ spectrum (22) is indeed the leading order for large ωt_m . Exact $1/f$ noise, with $\beta = 1$ and logarithmic time dependence [6], is not discussed here and left for a future work. In Secs. VII–IX we show that this result is not valid for arbitrarily large frequencies since then the scaling assumption breaks down.

We note that when $\omega t_m \gg 1$, the spectrum is controlled by the first term, which was determined by the nonanalytic expansion of the autocorrelation function when $\tau \ll t_m$. The oscillating behavior seen in Eq. (23) is a finite-measurement-time effect and is related to the autocorrelation function when

$\tau \sim t_m$. Thus, detecting these oscillations gives insight on the details of the underlying autocorrelation function. In fact, since $1/f^\beta$ spectrum is so common, yet its physical origin still remains unclear in many cases, the oscillating part of the spectrum might be a valuable tool for distinguishing between microscopic models. These oscillations depend only on the scaling variable ωt_m and are universal in that sense. In our examples below Eq. (22) works well also when $\omega t_m \approx 1$.

We note that when the spectrum is evaluated on the natural frequencies $\omega t_m = 2\pi n$, $n \in \mathbb{N}$, then according to Eq. (22) the power spectrum is characterized by two exponents: Υ and V . These are given in Table I for specific systems exhibiting aging. When we consider the continuous frequencies then, according to Eq. (23), the spectrum is quantified using three exponents Υ , V , and Λ describing the time and frequency dependence of the $1/f^\beta$ spectrum. Below we discuss three additional exponents, which characterize the process.

V. CRITICAL EXPONENTS AND SCALING RELATIONS

As mentioned in the Introduction, traditional theories of $1/f^\beta$ noise characterize the spectrum with a single exponent β . However, this is not sufficient as recent studies show [5,6,43,51]. We follow [51] and characterize the finite-time power spectra $S_{t_m}(\omega)$ with five power laws as follows: (i) the power spectrum frequency dependence $S(\omega) \sim \omega^{-\beta}$ for low frequencies, (ii) the power spectrum time dependence $S(\omega) \sim A_{t_m} \omega^{-\beta}$ where $A_{t_m} \sim t_m^{-z}$ for long times, (iii) the lower cutoff time dependence $\omega_{\min} \sim t_m^{-\eta}$, (iv) the power at zero frequency $S(0) \sim t_m^\mu$, and (v) the total measured power $\int_{1/t_m}^\infty S(\omega) d\omega \sim t_m^\delta$. In this section, we compute these exponents from the properties of the autocorrelation function. We will later consider three physical models where these

TABLE II. Summary of the scaling autocorrelation function exponents [see Eq. (20)] for the three systems discussed in Secs. VI–VIII. The first and second columns list the system and its relevant scaling exponent range.

Model	Exponent range	Υ	V	Λ
Single-file diffusion		1/2	1/2	-1/2
Blinking quantum dot–finite mean “on” time	$0 < \alpha < 1$	$2\alpha - 2$	$\alpha - 1$	$\alpha - 1$
Blinking quantum dot–infinite mean	$0 < \alpha < 1$	0	$1 - \alpha$	$-\alpha$
Logarithmic potential	$1 < \alpha < 3$	$2 - \alpha$	$2 - \alpha$	$1/2 - \alpha$

exponents are calculated explicitly; see Tables II and III for a summary.

We consider a process with an autocorrelation function with the scaling behavior (20). The critical exponent β which is determined by the power-law decay of the average power spectra in Eq. (22) is

$$\beta = 1 + V, \quad (24)$$

where $\beta \neq 1$. In addition, the aging exponent z which is related to the time decay is

$$z = V - \Upsilon, \quad (25)$$

so clearly $\beta = 1 + z + \Upsilon$. When $\beta = 1$, logarithmic time corrections are expected [6]. In an experimental situation the exponent Υ may be measured through the zero-frequency power as described in the next paragraph.

A. Zero-frequency power density and the exponent μ

To determine the exponent Υ , one may measure the spectrum at zero frequency, i.e., $\langle S_{t_m}(\omega = 0) \rangle = t_m \langle \bar{I}_{t_m}^2 \rangle$ where the time-averaged signal is $\bar{I}_{t_m} = \int_0^{t_m} I(t) dt / t_m$. Of course, the zero frequency cannot be considered part of the spectrum itself, at least not in the traditional sense, since in a finite time measurement one cannot detect a frequency shorter than $2\pi/t_m$. However, this does not imply that it cannot be measured, it is rather easy to do so. For a stationary process, $\langle S_{t_m}(0) \rangle$ is linearly dependent on the measurement time t_m . For a nonstationary process, its time dependence is related to the exponent Υ as follows.

When the ensemble-average autocorrelation function is scaled as Eq. (12), the power density at zero frequency

is

$$\langle S_{t_m}(\omega = 0) \rangle = 2t_m^{\Upsilon+1} \int_0^\infty dx \frac{\phi_{\text{EA}}(x)}{(1+x)^{\Upsilon+2}} \quad (26)$$

or, equivalently (after a change of variables),

$$\langle S_{t_m}(\omega = 0) \rangle = 2t_m^{\Upsilon+1} \int_0^1 dx \phi_{\text{EA}}\left(\frac{x}{1-x}\right). \quad (27)$$

The exponent μ is hence given by

$$\mu = 1 + \Upsilon. \quad (28)$$

Notice that the scaling relation $\mu = \beta - z$ is also valid. This relation was suggested in Ref. [51] in the context of blinking-quantum-dot models.

Remark. Equation (26) was already obtained in the context of a scaling Green-Kubo relation [54]. The scaling Green-Kubo formula expresses the relation between the diffusion coefficient of an enhanced diffusion process, and the scale invariant velocity autocorrelation function. The mean-squared displacement is equivalent to $t_m \langle S(0) \rangle$ which is the spectrum in zero frequency multiplied by the measurement time t_m .

B. Lower cutoff time dependence

The lower cutoff time dependence $\omega_{\min} \sim t_m^{-\eta}$ is defined by the transition frequency between the power-law decay $\langle S_{t_m}(\omega) \rangle_{\omega t_m \gg 1}$ and $\langle S_{t_m}(0) \rangle$. By comparing Eqs. (22) and (27), i.e., $\langle S_{t_m}(0) \rangle = A_V t_m^{\Upsilon-V} \omega_{\min}^{-1-V}$ where $A_V = 2\tilde{\alpha}_V \sin(\pi V/2) \Upsilon(1+V)$, we find

$$\omega_{\min} \sim t_m^{-1}. \quad (29)$$

We thus conclude that $\eta = 1$ for all processes with an autocorrelation function in the form of Eq. (12).

The existence of such a cutoff is required since a purely $1/f^\beta$ noise cannot exist in the range $0 < f < \infty$ for the following reasons. First, the power at zero frequency must be finite since $\langle \bar{I}_{t_m}^2 \rangle < \infty$, for every finite measurement time. Second, we expect the total power to be finite at every finite measurement time since

$$\int_{-\infty}^\infty d\omega \langle S_{t_m}(\omega) \rangle = 2\pi t_m^\Upsilon \varphi_{\text{TA}}(0), \quad (30)$$

even though Eq. (23) is not integrable in $[0, \infty)$. Notice that the sample spectrum is time dependent although its $1/f^\beta$ part might be time independent, e.g., if $\Upsilon = V$. Therefore, measuring $1/f^\beta$ noise, even time independent, does not contradict the finite power requirement. Equation (30) implies that $\langle S_{t_m}(\omega) \rangle$ is normalized, provided that $\varphi_{\text{TA}}(0)$ is finite,

TABLE III. Summary of the critical exponents for the three systems discussed in Secs. VI–VIII.

Model	Exponent range	β $S \sim \omega^{-\beta}$	z $S \sim t_m^{-z}$	η $\omega_{\min} \sim t_m^{-\eta}$	μ $S(0) \sim t_m^\mu$	δ $\int_{1/t_m}^{\omega_{\max}} S_{t_m}(\omega) d\omega$
Single-file diffusion		3/2	0	1	3/2	1/2
Blinking quantum dot–finite mean “on” time	$0 < \alpha < 1$	α	$1 - \alpha$	1	$2\alpha - 1$	$\alpha - 1$
Blinking quantum dot–infinite mean	$0 < \alpha < 1$	$2 - \alpha$	$1 - \alpha$	1	1	0
Logarithmic potential	$1 < \alpha < 2$	$3 - \alpha$	0	1	$3 - \alpha$	$2 - \alpha$
	$2 < \alpha < 3$	$3 - \alpha$	0	1	$3 - \alpha$	0

and since it is non-negative it satisfies the conditions for a normalized density [56].

C. Total power time dependence

For an ideal $1/f^\beta$ source, the total power of the process diverges since $\int_0^\infty \omega^{-\beta} d\omega = \infty$. If $\beta < 1$ ($\beta > 1$) the integral diverges due to the high- (low-) frequency limit. We should be mainly concerned with low frequency since the whole behavior of $1/f^\beta$ is found in that regime. Indeed, as we show below, there always exists a physical mechanism that leads to a cutoff at large frequencies. As was mentioned in Sec. V, the total measured power is characterized by the exponent δ , i.e., $\int_{1/t_m}^{\omega_{\max}} S(\omega) d\omega \sim t_m^\delta$, where we assume that ω_{\max} is time independent. As a result,

$$\int_{1/t_m}^{\omega_{\max}} S(\omega) d\omega \sim \omega_{\max}^{-\nu} t_m^{\gamma-\nu} + t_m^\gamma = \omega_{\max}^{-\nu} t_m^{-z} + t_m^{\mu-1}. \quad (31)$$

The exponent δ is accordingly given by

$$\delta = -\min(z, 1 - \mu). \quad (32)$$

Taking $\omega_{\max} \rightarrow \infty$ the total power time dependence scales as t_m^γ as is expected from Eq. (30).

For bounded processes, we expect that the total power will not increase as a function of time, namely, $\gamma \leq 0$. By contrast, in open (i.e., unbounded) processes, the total measured power may increase with measurement time, as for example single-file diffusion in infinite system, as we will discuss below.

VI. BASIC REQUIREMENTS FOR THE SPECTRAL DENSITY THEOREM

We now compare between the properties of Wienerian and aging power spectra clarifying the meaning of the latter. Stationary processes $I(t)$ and their power spectrum have the following properties:

- (i) $\langle I \rangle$ is a constant independent of time.
- (ii) $\langle I^2 \rangle$ is a constant independent of time and the correlation function $\langle I(t + \tau)I(t) \rangle$ is a function of τ only.
- (iii) The power spectrum is non-negative.
- (iv) The total power is

$$P_T = \int_{-\infty}^{\infty} S(\omega) d\omega = 2\pi \langle I^2 \rangle. \quad (33)$$

This well-known property is easily verified using the Wiener-Khinchin theorem.

- (v) The total power is

$$P_T = 2\pi \sum_{n=-\infty}^{\infty} \langle |a_n|^2 \rangle = 2\pi \langle I^2 \rangle, \quad (34)$$

where a_n is the Fourier amplitude $a_n = \int_0^{t_m} \exp(-i\omega_n t) I(t) dt / t_m$ and $\omega_n = 2\pi n / t_m$. Here, $\langle S(\omega) \rangle = t_m |a_n|^2$ in the limit of large t_m . See further discussion in Appendix A and in Ref. [1].

Properties (iii)–(v) are important, they show that the power spectrum is the distribution of the modes of the system, and that we may normalize the power spectrum. Indeed, in many cases the normalized power spectral density is considered, namely, $\langle S(\omega) \rangle / [2\pi \langle I^2 \rangle]$.

Our approach provides a non-Wienerian framework for the power spectrum. It is thus natural to ask how the above points translate to the nonstationary, non-Wienerian case.

- (i) $\langle I \rangle$ is a constant independent of time.
- (ii) Here, $\langle I(t + \tau)I(t) \rangle = t^\gamma \phi_{EA}(\tau/t)$ is the starting point. So, we get by definition

$$\langle I^2(t) \rangle = t^\gamma \phi_{EA}(0). \quad (35)$$

- (iii) The power spectrum $\langle S_{t_m}(\omega) \rangle \geq 0$ due the definition of the periodogram.
- (iv) We find

$$\begin{aligned} \int_{-\infty}^{\infty} \langle S_{t_m}(\omega) \rangle d\omega &= \frac{2\pi}{t_m} \left\langle \int_0^{t_m} I^2(t) dt \right\rangle \\ &= 2\pi \langle \overline{I^2} \rangle = 2\pi \varphi_{TA}(0). \end{aligned} \quad (36)$$

Here, the overline stands for a time average. The key to the interpretation of the power spectrum is Eq. (13) from which we find

$$\varphi_{TA}(0) = \lim_{x \rightarrow 0} x^{1+\gamma} \int_x^\infty dy \frac{\phi_{EA}(y)}{y^{2+\gamma}}. \quad (37)$$

Using L'Hôpital's rule we find

$$\varphi_{TA}(0) = \frac{\phi_{EA}(0)}{1 + \gamma}. \quad (38)$$

Thus, using Eqs. (35) and (36) the total power is

$$P_T = \int_{-\infty}^{\infty} S_{t_m}(\omega) d\omega = \frac{2\pi \langle I^2 \rangle}{1 + \gamma}. \quad (39)$$

Hence, exactly like the stationary theory, for scale invariant autocorrelation functions, the total power is given by $\langle I^2 \rangle$. Hence, it is fully justified to call $\langle S_{t_m}(\omega) \rangle$ the power spectral density. When $\gamma = 0$, the analogy is complete.

- (v) Also here, rule (34) holds, with P_T given in the previous item (see discussion in Appendix A with respect to filtering).

We hence see that even though the autocorrelation function is by definition far from being stationary, the main structure of power spectrum theory is left untouched, though now the power spectrum is dependent on the measurement time.

Since the aging spectrum is very different from the Wienerian one, we actually have two methods to present it (as shown all along this work). The spectrum of a $1/f^\beta$ noise source of the type discussed in this paper should be presented, if possible, using two plots: The first is $\langle S(\omega) \rangle$ versus ω where $\omega_n = 2\pi n / t_m$, this represents the *true spectrum* in the sense that Fourier modes in $(0, t_m)$ are discrete. As well known within this traditional presentation, $1/f^\beta$ noise presents an infrared divergence, $S(f) \sim f^{-\beta}$ which $\beta \geq 1$ implies naively that the total energy of the process is infinite (the low-frequency paradox of $1/f^\beta$ noise [5,48]). To gain better insight on this low-frequency behavior, we consider a second ‘‘spectrum’’ where $\langle S(\omega) \rangle$ is continuous in $0 \leq \omega < \infty$. This spectrum yields insights on the low-frequency behavior, namely, the oscillations of the spectrum and the zero-frequency component $\langle S(0) \rangle$. All these yield significant insight on the process, e.g., the exponents $\gamma, \nu, \Lambda, \beta, z, \eta, \mu$, and δ . By contrast, evaluating the spectrum at the natural frequencies yields only the $1/f^\beta$ component, which provides partial information on the spectrum, i.e., the exponents γ, β, z , and δ . We would like

to emphasize that all five exponents related to the spectrum, β , z , η , μ , and δ , can be evaluated from natural frequency data, provided that one adds one single measurement: the time-dependent behavior of $S_{t_m}(0)$. Three of them, β , z , and δ , can be evaluated even without information on the zero-frequency spectrum (then the cutoff is simply $1/t_m$). The advantage of the continuous spectrum is that it can give further information, for example, by the analysis of oscillations of the spectrum we may estimate Λ which yields information on the large argument behavior of the autocorrelation function. So, while $\langle S(\omega) \rangle$ on the natural frequencies $\omega_n = 2\pi n/t_m$ has the advantage of a clear interpretation in terms of Fourier modes (see, e.g., Kubo *et al.* [1]), the continuous spectrum gives insights on the underlying process which should not be ignored. The fact that the scaling autocorrelation function on which we base our analysis can be observed in a wide range of systems, beyond the specific examples discussed here, underlines the universality of our main results.

VII. BLINKING-QUANTUM-DOT MODEL

We next demonstrate the above results by studying a stochastic model for blinking quantum dots. A quantum dot is a nanocrystal that, when interacting with a continuous wave exciting laser field, switches at random times between on and off states [62,63]. Such a process is an example of a renewal process. To analyze such systems, we follow previous works (e.g., [22,50,64]) and define a two-state system, where $I(t) = 0$ is the state “off” and $I(t) = 1$ is “on.” Without loss of generality we choose the system to be initially in $I(0) = 1$. At each time t_n , the system switches to the other state alternately (“on” \rightarrow “off” or “off” \rightarrow “on”). The renewal times are $t_n = \sum_0^n \tau_i$ where $\{\tau_i\}$ are distributed according to the PDF $\psi(\tau)$ and n is the number of renewals until time t_n (see Fig. 2). We assume that the “on” and “off” times $\{\tau_i\}$ are uncorrelated. The

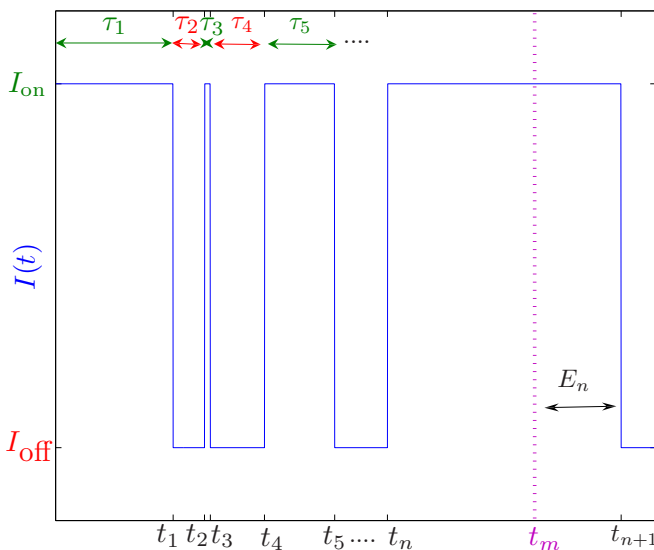


FIG. 2. A single realization of the signal $I(t)$ versus time (blue). $\{\tau_i\}$ are the sojourn times at each state: “on” (green) and “off” (red). $\{t_i\}$ are the renewal times, t_m is the measurement time, and E_n refers to the forward recurrence time.

“off” sojourn times are power-law distributed $\psi(\tau) \sim \tau^{-(1+\alpha)}$ with $0 < \alpha < 1$. For the “on” times we consider two cases. In the first one, the “on” times are distributed with infinite mean, e.g., a power-law distribution $\psi(\tau) \sim \tau^{-(1+\alpha)}$ [see the realization of $I(t)$ in Fig. 1 with $\alpha = 0.8$]. In the second case, we consider “on” times with a finite mean distribution, e.g., a power-law distribution with an exponentially decaying tail. Both cases were experimentally examined [51,65]. Such a system follows a power-law intermittency route to $1/f^\beta$ noise. This means that power-law waiting times in a substate of the system are responsible for the observed spectrum. This approach was suggested as a fundamental mechanism for $1/f^\beta$ noise in the context of intermittency of chaos and turbulence in the work of Manneville [66]. We note that the renewal process describes not only blinking dots, but also the trap model, a well-known model of glassy dynamics [7,21]. The connection between the two systems is the power-law waiting times in the microstates of the system.

A. Infinite mean “on” sojourn time distribution

In this model both “on” and “off” times are power-law distributed

$$\psi_{\text{off/on}}(\tau) \sim (\tau_0/\tau)^{1+\alpha}, \quad (40)$$

where τ_0 is a microscopic time scale, $\tau > \tau_0$, and $0 < \alpha < 1$ (e.g., see the experiment in [65]). We choose for both substates “on” and “off” the same exponent α for simplicity. Typical values of α in experiments are $0.5 < \alpha < 0.8$. This case was studied analytically before in Refs. [5,22,50,64,67,68].

The analytic formulas for the time- and ensemble-averaged autocorrelation function are given in [50], where t and τ are larger than τ_0 , positive and comparable:

$$\begin{aligned} \phi_{\text{EA}}(x) &= \frac{1}{2} - \frac{1}{4} \frac{\sin(\pi\alpha)}{\pi} B\left(\frac{x}{1+x}; 1-\alpha, \alpha\right), \\ \phi_{\text{TA}}(x) &= \frac{1}{4} + \frac{1}{4} \frac{\sin(\pi\alpha)}{\pi} \left[\frac{B(1-x; \alpha, 1-\alpha)}{1-x} \right. \\ &\quad \left. - \frac{1}{\alpha} \left(\frac{x}{1-x}\right)^{1-\alpha} \right], \end{aligned} \quad (41)$$

where $x = \tau/t$ and $B(z; a, b) \equiv \int_0^z dx (1-x)^{b-1} x^{a-1}$ is the incomplete beta function. In order to determine the power spectrum for this nonstationary process, we need to use the aging Wiener-Khinchin theorem (10) or (16) instead of Eq. (1).

We find by using Eqs. (16) and (41) (see derivation in Appendix C),

$$\langle S_{t_m}(\omega) \rangle / t_m = \frac{1}{4} \text{sinc}^2\left(\frac{\tilde{\omega}}{2}\right) + \frac{1}{2\tilde{\omega}} \text{Im}[M(1-\alpha, 2; i\tilde{\omega})], \quad (42)$$

where $\tilde{\omega} = \omega t_m$, $M(a, b; x)$ is the Kummer confluent hypergeometric function, and $\text{Im}[\dots]$ refers to its imaginary part. The $\text{sinc}^2(\dots)$ term is the contribution to the spectrum from a constant term. Equation (42) predicts the behavior of the power spectrum where $t_m \rightarrow \infty$ but $\tilde{\omega}$ remains finite.

1. $1/f^\beta$ noise

The average power spectrum of the signal $I(t)$, by using Eqs. (20), (22), and (41), is

$$\langle S_{t_m}(\omega) \rangle_{\omega t_m = 2\pi n} \approx \frac{\cos(\alpha\pi/2)}{2\Gamma(1+\alpha)} t_m^{\alpha-1} \omega^{\alpha-2}. \quad (43)$$

The same result is found by taking the limit of $\omega t_m \gg 1$ in Eq. (42). The aging Wiener-Khinchin theorem reproduces the result (43) that was found before, e.g., in Ref. [50]. To evaluate the oscillating behavior, we use Eq. (23) and find

$$\langle S_{t_m}(\omega) \rangle_{\omega t_m \gg 1} \approx \frac{\cos(\alpha\pi/2)}{2\Gamma(1+\alpha)} t_m^{\alpha-1} \omega^{\alpha-2} + \frac{t_m}{4} \text{sinc}^2\left(\frac{\omega t_m}{2}\right) - \frac{\cos[\omega t_m - \alpha\pi/2]}{2\Gamma(1-\alpha)\omega^{2+\alpha} t_m^{\alpha+1}}. \quad (44)$$

In Fig. 3, simulation results are compared with the exact analytic prediction (42) and excellent agreement is observed. Figure 3 further confirms the validity of the two approximated

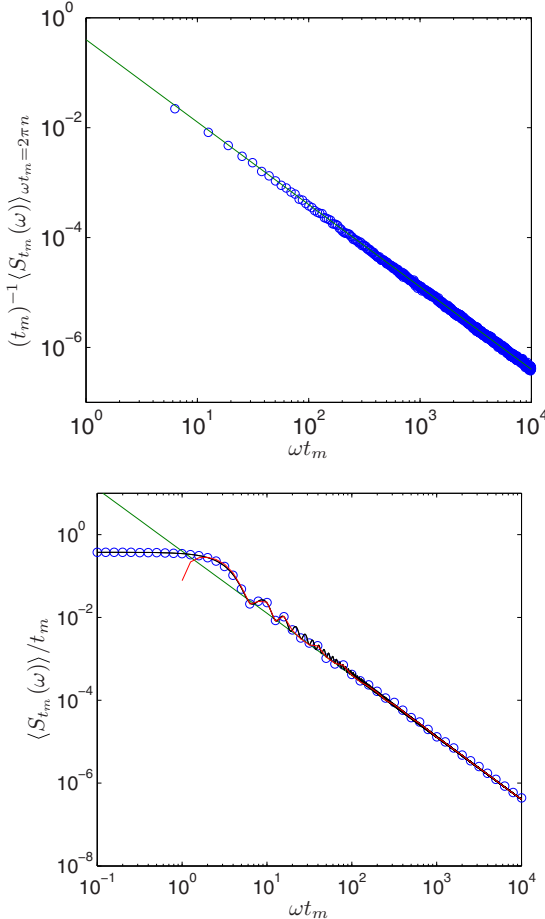


FIG. 3. Simulation results for a blinking-quantum-dot model where both distributions of “on” and “off” sojourn times are fat tailed [Eq. (40)] when $\alpha = 0.5$ at measurement time $t_m = 10^5$. In the upper panel, the spectrum is given at natural (discrete) frequencies $\omega t_m = 2\pi n$ and [compare to Eq. (43)] represented by the green line. In the lower panel, the power spectrum is taken at continuous frequencies, where complete analytic prediction is the black line [Eq. (42)]. The simulations method is given in Appendix C.

spectra: First, the $1/f^\beta$ noise (43) for discrete frequencies $\omega t_m = 2\pi n$ agrees well with the simulations when $n \in \mathbb{N}$. Moreover, the oscillatory behavior (44) for continuous frequencies presents a good agreement in the limit $\omega t_m \gg 1$.

2. Critical exponents

The critical exponent β , which is determined by the power-law decay of the average power spectra, is $\beta = 2 - \alpha$ for the infinite mean “on” sojourn time. The aging exponent which is related to the time decay is $z = 1 - \alpha$.

The averaged zero-frequency power spectrum is defined as $\langle S(\omega = 0) \rangle = t_m^{-1} \int_0^{t_m} dt_1 \int_0^{t_m} dt_2 \langle I(t_1)I(t_2) \rangle$. Using Eq. (41) we find

$$\langle S_{t_m}(0) \rangle = \frac{1}{4}(2 - \alpha)t_m, \quad (45)$$

hence, its related exponent is $\mu = 1$. The transition point between $\langle S_{t_m}(\omega) \rangle$ when $\omega \neq 0$ to the behavior at $\langle S_{t_m}(\omega = 0) \rangle$ is defined as the low-frequencies cutoff ω_{\min} :

$$\omega_{\min} = \left[\frac{2 \cos(\alpha\pi/2)}{\Gamma(1+\alpha)(1-\alpha)} \right]^{\frac{1}{2-\alpha}} t_m^{-1}. \quad (46)$$

Therefore, we find the exponent $\eta = 1$.

The highest frequency where $1/f^\beta$ appears, ω_{\max} , is related to the frequency at which the approximation (20) fails. Using the Laplace transform of the waiting time probability density function (PDF) $\hat{\psi}(u) \sim 1 - \Gamma(1-\alpha)(\tau_0 u)^\alpha$, such an approximation holds when $\omega \ll \omega_{\max} \sim \tau_0^{-1}$. The behavior of the total measured power is eventually

$$\int_{\omega_{\min}}^{\omega_{\max}} d\omega \langle S_{t_m}(\omega) \rangle \propto \text{const}. \quad (47)$$

We hence find $\delta = 0 = -\min(z = 1 - \alpha, 1 - \mu = 0)$ as expected.

B. Finite mean “on” sojourn time distribution

Now, we consider that the “on” sojourn times have a finite mean $\langle \tau \rangle$, while the “off” times are power-law distributed as the first case $\psi_{\text{off}}(\tau) \sim (\tau_0/\tau)^{1+\alpha}$ (see the measurements in [51]). In Laplace space ($s \rightarrow t$) we find for small s when $0 < \alpha < 1$

$$\begin{aligned} \hat{\psi}_{\text{on}}(s) &= 1 - \langle \tau \rangle s + \dots, \\ \hat{\psi}_{\text{off}}(s) &= 1 - a s^\alpha + \dots, \end{aligned} \quad (48)$$

where $a = \Gamma(1-\alpha)\tau_0^\alpha$. The ensemble-averaged autocorrelation function in the limit $\tau, t \rightarrow \infty$ scales as [22]

$$C(t, \tau) = \frac{\langle \tau \rangle^2}{a^2 \Gamma^2(\alpha)} (t\tau)^{\alpha-1}. \quad (49)$$

Using Eqs. (8) and (10), we obtain the power spectrum

$$\begin{aligned} \langle S_{t_m}(\omega) \rangle &= \frac{2\langle \tau \rangle^2 \pi \Gamma(1+\alpha) t_m^{2\alpha-1}}{\alpha a^2 4^\alpha \Gamma(\alpha)} \\ &\times {}_2\tilde{F}_3 \left[\frac{1+\alpha}{2}, \frac{\alpha}{2}; \frac{1}{2}, \frac{1}{2} + \alpha, 1 + \alpha; -\frac{\tilde{\omega}^2}{4} \right], \end{aligned} \quad (50)$$

where ${}_2\tilde{F}_3[a_1, a_2; b_1, b_2, b_3; z]$ is the regularized hypergeometric function (see Fig. 4).

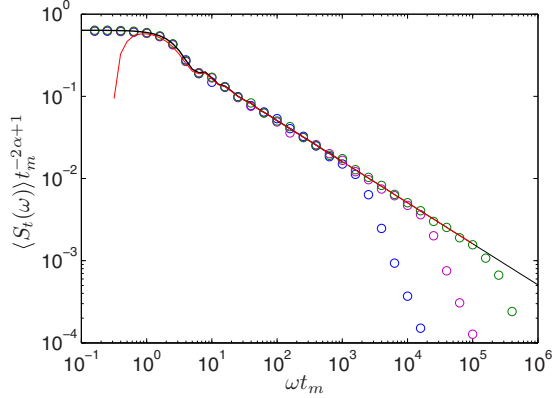


FIG. 4. The simulation results (circles) for the $\langle S_t(\omega) \rangle$ in the blinking-quantum-dot model with finite-mean “on” times and the power-law “off” times. We use $\alpha = 0.5$ at three different measurement times $t_m = 10^3$ (blue), $t_m = 10^4$ (pink), and $t = 10^5$ (green). The solid black line represents Eq. (50) and red line is Eq. (52). As we increase the measurement time, the simulations approach theoretical prediction.

We note that Eqs. (42) and (50) are valid only for finite $\tilde{\omega}$ even though Eq. (16) imposes no such restriction. For very large frequency, we expect to get nonscaling deviations since then the scale invariant autocorrelation function is not strictly valid for the Wiener-Khinchin theorem. For illustrations, see Fig. 4 where a different behavior emerges at large ω . This is a consequence of taking the autocorrelation function in the long-time limit, i.e., $t, \tau \rightarrow \infty$. Information about the autocorrelation function for short τ is necessary to find the behavior of the spectrum at high frequencies. A more detailed discussion will be published elsewhere [56]. However, Fig. 4 clearly illustrates that as we increase the measurement time the asymptotic behavior perfectly matches the theory.

1. $1/f^\beta$ noise

By using Eqs. (20), (22), and (49) we obtain

$$\langle S_t(\omega) \rangle_{\omega t_m = 2\pi n} \approx \frac{2\langle \tau \rangle^2 \cos(\pi\alpha/2)}{\Gamma(\alpha)a^{2\alpha}} t_m^{\alpha-1} \omega^{-\alpha}. \quad (51)$$

As in the infinite mean “on” times, the same result is found by taking the limit $\tilde{\omega} \gg 1$ in Eq. (50). In addition, we examine the oscillating behavior

$$\begin{aligned} \langle S_t(\omega) \rangle_{\omega t_m \gg 1} &\approx \frac{2\langle \tau \rangle^2 \cos(\pi\alpha/2)}{\Gamma(\alpha)a^{2\alpha}} t_m^{\alpha-1} \omega^{-\alpha} \\ &+ \frac{2\langle \tau \rangle^2 \Gamma(1+\alpha) \sin(\omega t_m - \alpha\pi/2)}{(1+\alpha)\Gamma^2(\alpha)a^2} \frac{1}{\omega^{1+\alpha} t_m^\alpha}. \end{aligned} \quad (52)$$

In Fig. 4, we compare the simulation results with the theory (50). The $1/f^\beta$ noise with oscillatory corrections [Eq. (52)] shows good agreement with numerical results for intermediate frequencies.

2. Critical exponents

From Eq. (43) we conclude that $\beta = \alpha$ and $z = 1 - \alpha$. The averaged zero-frequency power spectrum is then

$$\langle S_{t_m}(0) \rangle = \frac{\langle \tau \rangle^2}{\alpha \Gamma(2\alpha) a^2} t_m^{2\alpha-1}. \quad (53)$$

We therefore find $\mu = 2\alpha - 1$ for this case. This result is reasonable since the zero-frequency power is the squared-time-averaged signal $I(t)$ times the measurement time. The integral over $I(t)$ between zero and t_m is proportional to N_{t_m} times the average “on” time $\langle \tau \rangle$, where N_{t_m} is the number of renewals until time t_m . N_{t_m} itself is proportional to t_m^α , a well-known result in renewal theory [67]. Hence, we get $S_{t_m}(0) \propto t_m^{2\alpha-1}$.

Interestingly in this case the value of α changes the behavior of $\langle S_{t_m}(0) \rangle$, namely, if $\alpha > 1/2$ then $\langle S_{t_m}(0) \rangle$ increases in time, if $\alpha < 1/2$, it decreases in time, and when $\alpha = 1/2$ then $\langle S_{t_m}(0) \rangle$ is time independent.

The low-frequencies cutoff ω_{\min} is

$$\omega_{\min} = \left[\frac{2 \cos(\pi\alpha/2) \Gamma(2\alpha)}{\Gamma(\alpha)} \right]^{1/\alpha} t_m^{-1}. \quad (54)$$

Therefore, we find that in both cases the low-frequencies cutoff decays in time with the same exponent $\eta = 1$ and differs by a prefactor only.

The behavior of the total measured power is further

$$\int_{\omega_{\min}}^{\omega_{\max}} d\omega \langle S_{t_m}(\omega) \rangle \propto t_m^{-1}. \quad (55)$$

As a result, $\delta = \alpha - 1$. The decrease of the total power with measurement time is reasonable since the signal exhibits longer and longer “off” times, while the “on” times remain finite.

In Eq. (30) we showed that the total power is proportional to $t_m^\gamma \varphi_{\text{TA}}(0)$. This is true for the ideal process, where the scale invariant autocorrelation functions are valid for all t and τ , and then $\varphi_{\text{TA}}(0) < \infty$. We note that Eq. (49) gives $\varphi_{\text{TA}}(0) \rightarrow \infty$, hence, we cannot use this equation to evaluate $\varphi_{\text{TA}}(0)$. Generally, we should use $\int_0^\infty S(\omega) d\omega = \pi \langle C_{\text{TA}}(t_m, 0) \rangle$. Indeed, for this case the ensemble-averaged autocorrelation function is $C(t, \tau = 0) \propto t^{\alpha-1}$ as is given in [22]. Then, following Eqs. (9), (12), and (13), we find $C_{\text{TA}}(t, \tau = 0) \propto t^{\alpha-1}$ as well.

VIII. SINGLE-FILE DIFFUSION

The second example that we investigate is single-file diffusion. Single-file diffusion refers to the motion of particles in unidimensional systems, where the particles cannot pass each other, hence their ordering is preserved. We assume an infinite system, and we are interested in the displacement $x(t)$ of a tagged particle while all other particles play the role of a bath [69–71]. This kind of system can be used as a model for the motion of a single molecule in a crowded unidimensional environment such as a biological pore or channel [72,73], and experimental studies of physical systems such as zeolites [74] and colloid particles in confined topology [75] or optical tweezers [76].

We distinguish between two initial configurations of the bath: a thermal (equilibrium) initial condition [denoted as $(\dots)_{\text{uni}}$] and a nonthermal initial condition of equally spaced

particles [labeled $(\dots)_{\text{lat}}$]. The free particle diffusion coefficient is D and the average spacing between nearest particles is a . We note that the tagged particle is affected by the surrounding particles only at long times, i.e., $t \gg a^2/(2D)$. At shorter times $t \ll a^2/(2D)$ the tagged particle diffuses normally.

The autocorrelation functions have been evaluated in [26] and are given, for $t \gg a^2/(2D)$, by

$$C(t, \tau)_{\text{uni}} = a \sqrt{\frac{D}{\pi}} \sqrt{t} \left(\sqrt{1 + \frac{\tau}{t}} + 1 - \sqrt{\frac{\tau}{t}} \right), \quad (56)$$

$$C(t, \tau)_{\text{lat}} = a \sqrt{\frac{D}{\pi}} \sqrt{t} \left(\sqrt{2 + \frac{\tau}{t}} - \sqrt{\frac{\tau}{t}} \right).$$

By using Eq. (16) we find that the spectrum for the equilibrium initial configuration is

$$t_m^{-3/2} \sqrt{\frac{1}{Da^2}} \langle S_{t_m}(\omega) \rangle_{\text{uni}} = \frac{2 + \cos(\tilde{\omega})}{\sqrt{\pi} \tilde{\omega}^2} - \frac{1 + 2 \cos(\tilde{\omega})}{\sqrt{2} \tilde{\omega}^{5/2}} \mathcal{C} \left(\sqrt{\frac{2\tilde{\omega}}{\pi}} \right) + \frac{\sqrt{2}}{\tilde{\omega}^{5/2}} \mathcal{S} \left(\sqrt{\frac{2\tilde{\omega}}{\pi}} \right) [-\tilde{\omega} + \sin(\tilde{\omega})], \quad (57)$$

where the Fresnel functions $\mathcal{C}(u)$ and $\mathcal{S}(u)$ are defined as

$$\mathcal{C}(u) = \int_0^u \cos(\pi t^2/2) dt, \quad (58)$$

$$\mathcal{S}(u) = \int_0^u \sin(\pi t^2/2) dt.$$

For the lattice initial condition, we obtain

$$t_m^{-3/2} \sqrt{\frac{1}{Da^2}} \langle S_{t_m}(\omega) \rangle_{\text{lat}} = \frac{\sqrt{2} + \cos(\tilde{\omega})}{\sqrt{\pi} \tilde{\omega}^2} - \frac{\cos(2\tilde{\omega})}{\sqrt{2} \tilde{\omega}^{5/2}} \left[\mathcal{C} \left(\sqrt{\frac{4\tilde{\omega}}{\pi}} \right) - \mathcal{C} \left(\sqrt{\frac{2\tilde{\omega}}{\pi}} \right) \right] + \frac{\sin(2\tilde{\omega})}{\sqrt{2} \tilde{\omega}^{5/2}} \left[\mathcal{S} \left(\sqrt{\frac{2\tilde{\omega}}{\pi}} \right) - \mathcal{S} \left(\sqrt{\frac{4\tilde{\omega}}{\pi}} \right) \right] + \frac{\sqrt{2}}{\tilde{\omega}^{3/2}} \left[\tilde{\omega} \mathcal{S} \left(\sqrt{\frac{2\tilde{\omega}}{\pi}} \right) - \mathcal{C} \left(\sqrt{\frac{2\tilde{\omega}}{\pi}} \right) \right]. \quad (59)$$

As we see in Fig. 5, these results are confirmed by simulations. The simulation method is described in Ref. [26]. As in the blinking-quantum-dot model we have assumed a scaling form of the autocorrelation function (56), which works in the limit of large time. Information on the autocorrelation function for short times is needed to estimate the very high-frequency limit of the spectrum. Hence, the deviations at high frequencies in Fig. 5 are expected. As the measurement time is increased, the spectrum plotted as a function of $\tilde{\omega}$ perfectly approaches the predictions of our theory (see also the following example and Fig. 6).

By using Eqs. (20) and (22), we further find that the power spectrum corresponding to the random displacement $x(t)$ reads

$$\langle S_{t_m}(\omega) \rangle_{\omega t_m = 2\pi n}^{\text{uni}} = \langle S_{t_m}(\omega) \rangle_{\omega t_m = 2\pi n}^{\text{lat}} = \sqrt{\frac{a^2 D}{2}} \omega^{-3/2}. \quad (60)$$

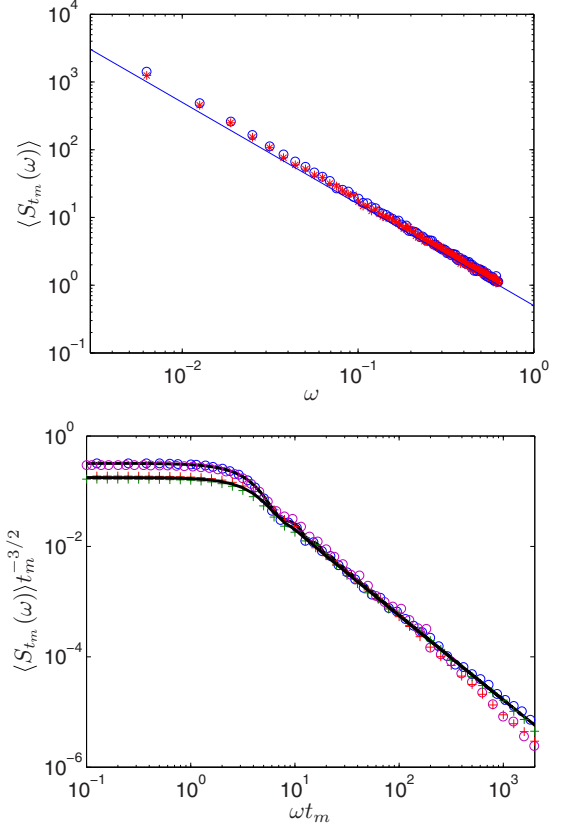


FIG. 5. The simulation results for single-file diffusion for the two initial conditions. Upper panel: the spectrum $\langle S_{t_m}(\omega) \rangle$ versus the natural frequencies $\omega = 2\pi n/t_m$, where $t_m = 10^3$ and $n \in \mathbb{N}$ for two initial conditions, uniform (blue circles) and equidistance (red dots). For such a presentation of the power spectrum, there is no distinction between two initial configurations. Lower panel: $\langle S_i(\omega) \rangle_{\text{uni}}$ (circles) at measurement times $t = 10^3$ (blue) and $t = 10^2$ (pink), and $\langle S_i(\omega) \rangle_{\text{lat}}$ (crosses) at measurement times $t = 10^3$ (green) and $t = 10^2$ (red). The solid black lines represent the analytic prediction Eqs. (57) and (59). The diffusion constant D and the average distances between particles a are taken to be $D = 0.5$ and $a = 1$. Deviations from theory at high frequencies are expected as explained in the text. They disappear as we take the measurement time to be long.

In the limit $\omega t_m = 2\pi n \gg 1$, the power spectrum seems to be time independent. However, we note that the spectrum $\langle S_{t_m}(\omega) \rangle$ remains time dependent. Hence, for every finite time t_m , the total power is finite because of the low-frequency cutoff at $\omega \sim 1/t_m$ (see Sec. V C). Moreover, measurements of the spectrum $\langle S_{t_m}(\omega) \rangle$ made without knowledge of initial conditions would be consistent within the range of frequencies allowed by the limited observation time. In other words, the spectrum in the high-frequencies limit $\omega \gg 1/t_m$ is not affected by the initial condition, although the process is nonstationary.

A. Critical exponents for single-file diffusion

From Eq. (60) we observe that $\beta = 3/2$ and $z = 0$ for both cases. Calculating $\langle S_{t_m}(0) \rangle$ by substituting $\omega = 0$ in Eq. (10)

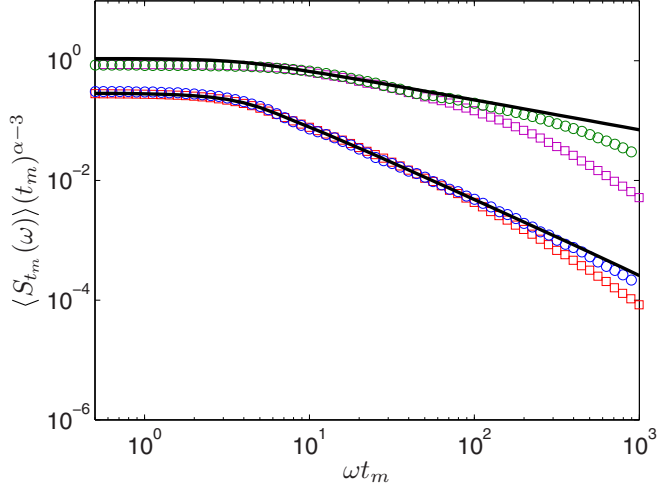


FIG. 6. The simulation results for the diffusion in a logarithmic potential when $D = 0.4$, at measurement times $t_m = 500$ (red squares) and $t_m = 2000$ (blue circles) and when $D = 0.25$, at measurement times $t_m = 500$ (pink squares) and $t_m = 2000$ (green circles). The black solid lines represent Eq. (68).

yields

$$\langle S_{t_m}(0) \rangle_{\text{uni}} = \sqrt{\frac{Da^2}{\pi}} \frac{2}{5} t_m^{3/2}, \quad (61)$$

$$\langle S_{t_m}(0) \rangle_{\text{lat}} = \sqrt{\frac{Da^2}{\pi}} \frac{8}{15} (\sqrt{2} - 1) t_m^{3/2}.$$

We may then conclude that $\mu = 3/2$ for both initial conditions. The low-frequency cutoff is furthermore found to be

$$\omega_{\text{min}}^{\text{uni}} = \left(\frac{25\pi}{8} \right)^{1/3} t_m^{-1}, \quad (62)$$

$$\omega_{\text{min}}^{\text{lat}} = \left(\frac{15\sqrt{\pi}}{8(2-\sqrt{2})} \right)^{2/3} t_m^{-1}$$

and consequently $\eta = 1$. The total measured power diverges here with time, i.e.,

$$\int_{\omega_{\text{min}}}^{\omega_{\text{max}}} \langle S_{t_m}(\omega) \rangle d\omega \sim t_m^{1/2} \quad (63)$$

for both initial configurations. As expected, the total power diverges since the displacement $x(t)$ is unbounded, even though for every finite time the total power is finite.

IX. BROWNIAN MOTION IN A LOGARITHMIC POTENTIAL

The third model that we consider is a Langevin equation with a logarithmic binding potential. Such a case is related, for example, to optical lattices, where x is the momentum [24,77]. It further describes the denaturing of DNA [78], Manning condensation on a polymer [79], or vortex dynamics [80]. Such a case is interesting since it is “weakly” bound and hence may exhibit different properties than free Brownian motion or Langevin dynamics in a harmonic potential [23,81].

The Langevin equation describes the temporal evolution of the variable x in a logarithmic binding potential for large x ,

$$\xi \frac{dx}{dt} + \frac{dU(x)}{dx} = \eta(t), \quad (64)$$

where ξ is a friction coefficient (we took a unit mass) and $\eta(t)$ is the white noise with zero mean, satisfying the fluctuation-dissipation relation. We assume that the potential is of the form

$$U(x) = \frac{1}{2} U_0 \ln(1 + x^2), \quad (65)$$

where the constant U_0 is related to the depth of the potential. In equilibrium, the PDF of x is $P_{eq}(x) \sim \exp[-U(x)/k_B T]$ due to the Boltzmann theorem, therefore, we find $P_{eq}(x) \sim (1 + x^2)^{-U_0/2k_B T}$, i.e., x has infinite variance when $1 < U_0/k_B T < 3$. We introduce the parameter α :

$$\alpha = \frac{U_0}{2k_B T} + \frac{1}{2} \quad (66)$$

and define a diffusion constant through the fluctuation-dissipation relation $D = k_B T/\xi$.

The autocorrelation function for the case where $\alpha > 1$ is given in [23], where both t and τ are assumed to be large:

$$C(t, \tau) \approx \frac{\sqrt{\pi}(4Dt)^{2-\alpha}}{Z\Gamma(\alpha)\Gamma(1+\alpha)} x^{2-\alpha} \int_0^\infty dy e^{-y^2} y^2 \times {}_1F_1\left(\frac{3}{2}, \alpha + 1, y^2\right) \Gamma(\alpha, y^2 x), \quad (67)$$

where $x = \tau/t$. Then, by using Eqs. (10) and (13), we find the spectrum

$$\langle S_{t_m}(\omega) \rangle = t_m^{3-\alpha} \frac{2\sqrt{\pi}(4D)^{2-\alpha}}{Z\Gamma(\alpha)\Gamma(\alpha+1)} \int_0^1 dx x^{3-\alpha} \cos(\tilde{\omega}x) \times \int_{\frac{x}{1-x}}^\infty dy y^{-2} \int_0^\infty dz e^{-z^2} y^2 \times {}_1F_1\left(\frac{3}{2}, \alpha + 1, z^2\right) \Gamma(\alpha, z^2 y). \quad (68)$$

This is computed numerically by first evaluating the integral over y explicitly and then evaluating the remaining two integrals numerically by using *Mathematica* where the upper boundary for the z integral is taken to be 10^5 instead of ∞ . The numerical results for $\alpha = 1.75$ ($D = 0.4$) and $\alpha = 2.5$ ($D = 0.25$) present good agreement with Langevin simulation results for not too large frequencies (see Fig. 6). Initially, the particle is situated at the origin $x(t=0) = 0$. Therefore, at short time the particle is not affected by the logarithmic tail of the potential. We thus expect a deviation from theory at high frequencies.

We obtain for $1 < \alpha < 2$ in the limit $x \ll 1$

$$C(t, \tau) \approx \frac{\sqrt{\pi}(4Dt)^{2-\alpha}}{Z\Gamma(\alpha)\Gamma(1+\alpha)} \left[\frac{\Gamma(\alpha+1)}{\sqrt{\pi}(2-\alpha)} + \frac{\sqrt{\pi}\Gamma(\alpha-2)\Gamma(\alpha+1)\Gamma(\alpha)}{4\Gamma^2(\alpha-\frac{1}{2})} x^{2-\alpha} \right], \quad (69)$$

where $Z = \sqrt{\pi}\Gamma(\alpha-1)/\Gamma(\alpha-1/2)$ is a normalization constant. For $2 < \alpha < 3$, the autocorrelation function in the limit

$\tau \ll t$ is stationary [23]

$$C(t, \tau) \approx \frac{\pi \Gamma(\alpha - 2)(4D\tau)^{2-\alpha}}{4Z\Gamma^2(\alpha - \frac{1}{2})}. \quad (70)$$

The corresponding power spectrum in discrete frequencies $\omega t_m = 2\pi n \gg 1$ for both cases $1 < \alpha < 2$ and $2 < \alpha < 3$ is, moreover,

$$\begin{aligned} \langle S_{t_m}(\omega) \rangle_{\omega t_m = 2\pi n} &= 2 \sin\left(\frac{\pi\alpha}{2}\right) \Gamma(3 - \alpha) \\ &\times \left[-\frac{\pi \Gamma(\alpha - 2)(4D)^{2-\alpha}}{4Z\Gamma^2(\alpha - 1/2)} \right] \omega^{\alpha-3}. \end{aligned} \quad (71)$$

We conclude that for both cases $1 < \alpha < 2$ and $2 < \alpha < 3$, the critical exponents are $\beta = 3 - \alpha$, $z = 0$, $\eta = 1$, and $\mu = 3 - \alpha$. The total measured power, for both cases, is

$$\int_{\omega_{\min}}^{\omega_{\max}} \langle S_{t_m}(\omega) \rangle d\omega \propto \text{const} + t_m^{2-\alpha}, \quad (72)$$

where $\omega_{\min} \sim 1/t_m$ and ω_{\max} is time independent. When $1 < \alpha < 2$, the total power increases with the time t_m , i.e., it diverges when $t_m \rightarrow \infty$, since this case corresponds to high temperature or shallow potential ($1 < U_0/k_B T < 3$) and thus the particle exhibits subdiffusion. When $2 < \alpha < 3$ (i.e., $3 < U_0/k_B T < 5$) we find that the total measured power in the frequencies range $(\omega_{\min}, \omega_{\max})$ converges to a constant, i.e., effectively the particle is bound. Therefore, its critical exponents are $\eta = 2 - \alpha$ for $1 < \alpha < 2$ and $\eta = 0$ for $2 < \alpha < 3$.

X. SUMMARY AND DISCUSSION

We have extended the Wiener-Khinchin theorem to non-stationary spectra by deriving two general relations between time- and ensemble-averaged autocorrelation functions and the aging power spectrum [34,35]. Just like the original Wiener-Khinchin theorem, it is by itself not a prediction for any specific system but rather a general connection between different properties (spectrum and correlation function) of the same system. The connection to the real system is then established by specifying the correlation function from a model and comparing it to the observed spectrum. We have moreover established the generic occurrence of $1/f^\beta$ noise for nonanalytic ensemble-averaged autocorrelation functions and derived the corresponding five critical exponents. We have evaluated these exponents for three models: blinking quantum dot, single-file diffusion, and diffusion in a logarithmic potential. The nonstationary spectrum retains all the important properties of the stationary one, in particular its interpretation as a density of Fourier modes.

We emphasize that the five exponents are not adjustable parameters but general features of the spectrum, which are fixed by the underlying microscopic theory. They are thus measurable observables, although the relevant variable should change over several orders of magnitude for a reliable estimation. Importantly, the exponents satisfy scaling relations and are thus not independent. In particular, for a process with constant variance, i.e., $C(t; \tau = 0) = \text{const}$ so $\Upsilon = 0$, these five exponents are determined by a single exponent V . For example, in the blinking-quantum-dot model with

infinite mean ‘‘on’’ times the latter exponent V is related to α which describes the power-law decay of the sojourn time. For processes with a time-dependent variance, namely $\Upsilon \neq 0$, only two parameters Υ and V determine the five exponents. We hope that our work will promote measurements of the different exponents of the $1/f^\beta$ spectrum since they reveal the true complexity of the observed phenomena.

The nonstationarity of the autocorrelation function does not necessarily imply that the spectrum in the $1/f^\beta$ regime is time dependent. Indeed, we have found that the $1/f^\beta$ spectrum of single-file diffusion and diffusion in a logarithmic potential are time independent. This happens because in these models, $\Upsilon = V$. Namely, the property of the autocorrelation function determines if the aging exponent z is zero or not. Therefore, by measuring time-independent $1/f^\beta$ noise, one cannot conclude that the process is stationary. This is well known for Brownian motion where the underlying process is nonstationary and the power spectrum is of the f^{-2} type. One way to reveal the nonstationarity is to present the data as $S/(t_m^{\Upsilon+1})$ versus $\tilde{\omega} = \omega t_m$ and see if a scaling solution is found. Another way is to search for the oscillations [see Eq. (23)].

In addition, we have shown how the power spectrum for the single-file system depends on the initial condition. This theme could be further investigated, for example, in KPZ models [33], or when the measurement of blinking dots does not start at the beginning of the process, i.e., the effect of a waiting time on the power spectrum is important [10,56,82].

ACKNOWLEDGMENT

This work was supported by the Israel Science Foundation.

APPENDIX A: RELATION OF THE AGING POWER SPECTRUM TO FOURIER MODES

Following [1] we consider a signal $I(t)$ which is observed over an interval $[0, t_m]$. Expand $I(t)$ in a Fourier series as

$$I(t) = \sum_{n=-\infty}^{\infty} a_n e^{i\omega_n t}, \quad (A1)$$

where the natural frequencies are defined $\omega_n = 2\pi n/t_m$, and the Fourier coefficients are

$$a_n = \frac{1}{t_m} \int_0^{t_m} I(t) e^{-i\omega_n t} dt, \quad (A2)$$

then, $I_{t_m}(\omega) = a_n t_m$ (see Sec. II in the main text). We define the spectrum for finite time as

$$\langle S_{t_m}(\omega) \rangle \equiv t_m \langle |a_n|^2 \rangle, \quad (A3)$$

where the measurement time t_m is assumed to be long.

We consider the blinking-quantum-dot model with long waiting time. Thus, the ensemble-averaged signal is simply a constant $\langle I(t) \rangle = 1/2$ (when starting in the ‘‘on’’ state this is valid in the long time limit [22]). The average Fourier coefficient then is

$$\langle a_n \rangle = \langle I \rangle \delta_{n0}. \quad (A4)$$

When a suitable filter is used, one may select a large number of the Fourier modes related to frequencies lying in the interval

$\Delta\omega$, and hence observe a smooth power spectral density:

$$S_{t_m}(\omega)\Delta\omega = \left(\sum_{\omega_n \in \Delta\omega} a_n \right)^2 = \sum_n |a_n|^2 + \sum_n \sum_{m \neq n} a_n a_m^*, \quad (\text{A5})$$

where the number of modes in an interval $\Delta\omega$ is $t_m \Delta\omega / (2\pi)$. To recover Eq. (A3), one should prove that the Fourier coefficients $\{a_n\}$ are mutually independent, i.e.,

$$\langle a_n a_m^* \rangle = \langle a_n \rangle \langle a_m^* \rangle = 0, \quad (\text{A6})$$

where $n \neq m$ (a topic left for future work). The last equality is a direct outcome of Eq. (A4).

1. Zero-frequency contribution

We briefly remind the reader of some basic properties of Wienerian processes, using an example. Consider a process $I(t)$ with a stationary autocorrelation function

$$\langle I(t)I(t+\tau) \rangle = [\langle I^2 \rangle - \langle I \rangle^2]e^{-\tau} + \langle I \rangle^2. \quad (\text{A7})$$

Following the Wiener-Khinchin theorem [Eq. (1)], we obtain the spectrum

$$\langle S(\omega) \rangle = 2\pi \langle I \rangle^2 \delta(\omega) + [\langle I^2 \rangle - \langle I \rangle^2] \frac{2}{1 + \omega^2}. \quad (\text{A8})$$

In experimental situations, the zero-frequency power is not usually reported in the total power estimation. Therefore, we expect to observe

$$H^+ = \int_{0^+}^{\infty} S(\omega) d\omega = \pi [\langle I^2 \rangle - \langle I \rangle^2]. \quad (\text{A9})$$

Including the zero point gives

$$H^- = \int_{0^-}^{\infty} S(\omega) d\omega = \pi [\langle I^2 \rangle + \langle I \rangle^2]. \quad (\text{A10})$$

Now, we have two ways to estimate $\langle I^2 \rangle$ from the power spectrum. The first one is to shift the stationary process $I(t)$ in such a way that $\langle I \rangle = 0$. The second one is to use the total power of a stationary process following the Wiener-Khinchin theorem [1]

$$\int_0^{\infty} \langle S(\omega) \rangle d\omega = \frac{1}{2} \int_{-\infty}^{\infty} \langle S(\omega) \rangle d\omega = \pi C(0) = \pi \langle I^2 \rangle, \quad (\text{A11})$$

where $\langle S(\omega) \rangle$ is an even function of frequency.

2. Continuous versus natural-frequencies spectrum

In its discrete form, one may compute by the Euler-Maclaurin formula

$$\int_0^{\infty} \langle S_{t_m}(\omega) \rangle d\omega \approx \sum_{n=1}^{\infty} \langle S_{t_m}(\omega_n) \rangle \Delta\omega + \frac{1}{2} \Delta\omega \langle S_{t_m}(0) \rangle, \quad (\text{A12})$$

where ω_n are the natural frequencies defined above. Using $S(0)\Delta\omega = |a_0|^2$ and $S(\omega_n)\Delta\omega = |a_n|^2$ we find the total power

$$\int_0^{\infty} \langle S(\omega) \rangle d\omega \approx 2\pi \left(\sum_{n=1}^{\infty} \langle |a_n|^2 \rangle + \frac{1}{2} \langle |a_0|^2 \rangle \right). \quad (\text{A13})$$

Following Parseval's identity

$$\sum_{n=-\infty}^{\infty} |a_n|^2 = \frac{1}{t_m} \int_0^{t_m} |I(t)|^2 dt \quad (\text{A14})$$

and symmetry, i.e., $a_n = a_{-n}$, we find

$$\sum_{n=1}^{\infty} \langle S(\omega_n) \rangle \Delta\omega + \frac{1}{2} \Delta\omega \langle S(0) \rangle = \pi \frac{1}{t_m} \int_0^{t_m} \langle |I(t)|^2 \rangle dt. \quad (\text{A15})$$

For a stationary process, the mean-squared displacement is time independent $\langle I^2 \rangle = C(0)$ and $\langle |a_0|^2 \rangle = \langle I \rangle^2$. Further, from ergodicity and (A14), $\sum |a_n|^2 = \langle I^2 \rangle$, therefore,

$$\sum_{n=1}^{\infty} \langle S(\omega_n) \rangle \Delta\omega = \pi (\langle I^2 \rangle - \langle I \rangle^2) = \pi C(0) - \pi \langle I \rangle^2, \quad (\text{A16})$$

i.e., the total spectrum measurement provides the variance of the signal.

In a nonstationary process, we obtain

$$\begin{aligned} \sum_{n=1}^{\infty} \langle S_{t_m}(\omega_n) \rangle \Delta\omega &= \pi \overline{\langle I_{t_m}^2 \rangle} - \pi \langle \overline{I_{t_m}} \rangle^2 \\ &= \pi t_m^\Upsilon \varphi_{\text{TA}}(0) - \pi \langle \overline{I_{t_m}} \rangle^2, \end{aligned} \quad (\text{A17})$$

where the last equality is based on the scaling assumption (9), i.e., $\overline{\langle I_{t_m}^2 \rangle} = t_m^\Upsilon \varphi_{\text{TA}}(0)$ and $\langle \overline{(\cdot)} \rangle$ is the time average defined as

$$\langle |a_0|^2 \rangle = \langle \overline{I_{t_m}} \rangle^2 = \left\langle \left[\frac{1}{t_m} \int_0^{t_m} I(t) dt \right]^2 \right\rangle. \quad (\text{A18})$$

In this case,

$$\sum_{n=-\infty}^{\infty} \langle |a_n|^2 \rangle = \frac{1}{t_m} \int_0^{t_m} \langle |I(t)|^2 \rangle dt = t_m^\Upsilon \varphi_{\text{TA}}(0). \quad (\text{A19})$$

We conclude that the time-dependent spectrum in its discrete form conserves the basic properties one expects the power spectrum to fulfill.

3. Illustration in blinking-quantum-dot model

We use the blinking-quantum-dot model to demonstrate numerically the estimation of the total power. Here, we present three methods of estimating the autocorrelation function from the power spectrum. We compare our results with the analytic results (see Fig. 7). Summing over the natural frequencies $\omega_n = 2\pi n / t_m$ where $n \in \mathbb{N}$,

$$\begin{aligned} P_{\text{exact}} &= \frac{1}{2} \sum_{n=-\infty}^{\infty} \langle S_{t_m}(\omega_n) \rangle \Delta\omega \\ &= \sum_{n=-\infty}^{\infty} \langle S_{t_m}(\omega_n) \rangle \frac{\pi}{t_m} = \pi/2, \end{aligned} \quad (\text{A20})$$

where in this model $\phi_{\text{EA}}(0) = \varphi_{\text{TA}}(0) = \pi/2$ and $\Upsilon = 0$ [see Eq. (41)].

The first method of evaluation of the total power is using the approximate spectrum (43) for $\langle S_{t_m}(\omega) \rangle$. It gives

$$P^I = \frac{\cos\left(\frac{\pi\alpha}{2}\right) (2\pi)^{\alpha-2} \zeta(2-\alpha)}{2\Gamma(1+\alpha)} + \frac{\pi}{4} (2-\alpha), \quad (\text{A21})$$

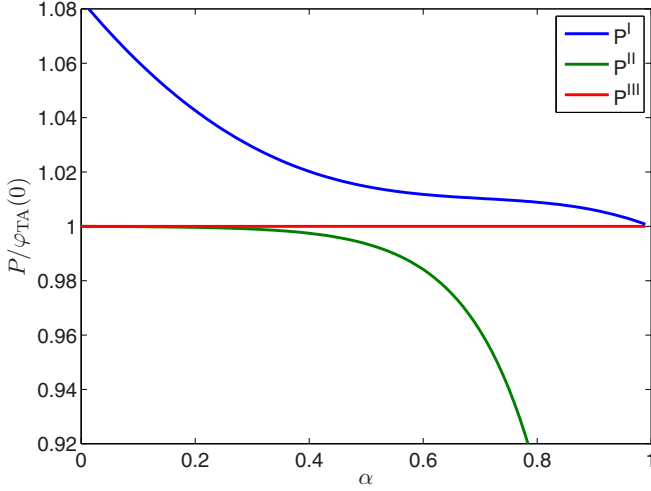


FIG. 7. Comparison between the three estimation methods with the exact value of the total power in the blinking-quantum-dot model.

where $\zeta(k) = \sum_{n=1}^{\infty} n^{-k}$ is the Riemann zeta function. The last term $\pi(2 - \alpha)/4$ is related to the contribution from $n = 0$. The deviation from the exact value (A20) may be caused by the deviations of the approximate natural frequencies spectrum (43) from the exact spectrum (42) for small n . It means that the $1/f$ noise formula (43) is not sufficient for a precise estimate of the total power (see Fig. 7).

As a second method for the estimation of the total power one may use the exact expression for the spectrum (42). The problem with this method is that there is no analytic expression for the infinite summation. To proceed, we use a cutoff $\omega_N = 2\pi N/t_m$, where $N = 10^3$, for the large frequencies:

$$P^{II} = \sum_{n=1}^{10^3} \left\{ \frac{\text{sinc}^2(\pi n)}{4} + \frac{\text{Im}[M(1 - \alpha; 2; 2i\pi n)]}{4\pi n} \right\} + \frac{\pi(2 - \alpha)}{4}. \quad (\text{A22})$$

A large deviation from the exact value is observed when α is larger than ≈ 0.7 since, when α approaches 1, the terms $\langle S_{t_m}(\omega_n) \rangle$ at $n > N$ contribute to the total power.

The third method is a combination of the two previous ones:

$$P^{III} = \sum_{n=1}^{10^3} \left\{ \frac{\text{sinc}^2(\pi n)}{4} + \frac{\text{Im}[M(1 - \alpha; 2; 2i\pi n)]}{4\pi n} \right\} + \frac{\cos(\frac{\pi\alpha}{2})(2\pi)^{\alpha-2}}{2\Gamma(1 + \alpha)} \sum_{n=10^3+1}^{\infty} n^{-2+\alpha} + \frac{\pi}{4}(2 - \alpha). \quad (\text{A23})$$

Comparing this estimation to the exact result $P_{\text{exact}} = \pi/2$ we find deviations of 0.005%. Comparison between the three methods is given in Fig. 7. We use *Mathematica* for the numerical estimation of the summations.

APPENDIX B: ON EQ. (11)

We here show how to estimate the autocorrelation function from the power spectrum. Equation (10) in the discrete

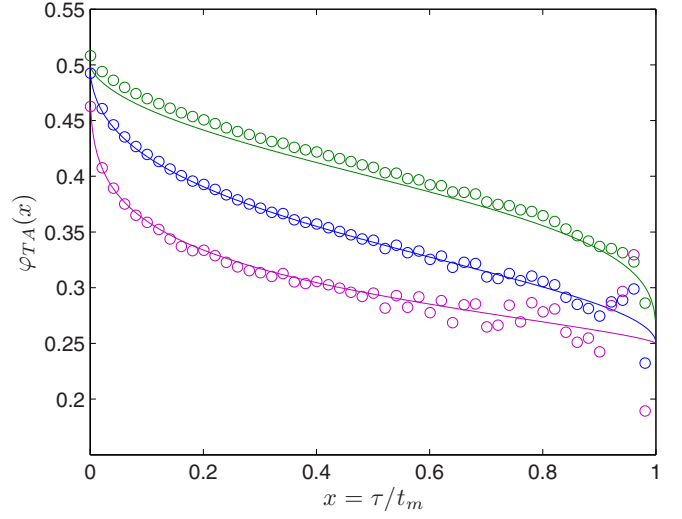


FIG. 8. The simulation results (open circles) for Eq. (B3) in the blinking-quantum-dot process with heavy tailed PDF sojourn times [Eq. (40)]. We examine three different exponents: $\alpha = 0.3$ (upper, green), $\alpha = 0.5$ (middle, blue), and $\alpha = 0.8$ (lower, pink). The solid lines represent the theory of time-averaged autocorrelation function [Eq. (41)]. The measurement time is 10^5 and the ensemble average was taken over 10^4 realizations.

form is

$$\langle S_{t_m}(\omega) \rangle \approx 2t_m^{\gamma+1} \sum_{n=1}^{N-1} (1 - n\Delta x) \varphi_{\text{TA}}(n\Delta x) \cos(\omega t_m n\Delta x) + t_m^{\gamma+1} \varphi_{\text{TA}}(0) \Delta x, \quad (\text{B1})$$

where we use the Euler-Maclaurin formula with the discrete variable $x_n = n\Delta x$ and $\Delta x = 1/N$ where N is large. Now, we multiply by $\cos(\omega t_m j\Delta x)$ and integrate over frequencies

$$\int_0^{\pi/(t_m\Delta x)} d\omega \cos(\omega t_m n\Delta x) \langle S_{t_m}(\omega) \rangle \approx \pi t_m^{\gamma} (1 - n\Delta x) \varphi_{\text{TA}}(n\Delta x), \quad (\text{B2})$$

where $n \neq 0$. Therefore, using $\tilde{\omega} = \omega t_m$, we obtain

$$\frac{1}{\pi(1-x)} \int_0^{N\pi} d\tilde{\omega} \cos(\tilde{\omega}x) \langle S_{t_m}(\tilde{\omega}) \rangle \approx t_m^{\gamma+1} \varphi_{\text{TA}}(x). \quad (\text{B3})$$

Now, we would like to decrease the x steps of the numeric integration for a certain measurement time t_m , or equivalently increasing N . Where $N \rightarrow \infty$ we recover Eq. (11) in the text.

In Fig. 8, we show the estimation of the time-averaged autocorrelation function for a blinking-quantum-dot model where the sojourn times $\{\tau_i\}$ are distributed with the PDF Eq. (40). We first find the power spectrum using the method presented in Appendix C. We then apply Eq. (B3) to our “experimental” data to find $\varphi_{\text{TA}}(x)$ which is presented in Fig. 8.

The ensemble-averaged autocorrelation function might be found by Eq. (19), using the measured sample spectrum directly. Another method to obtain $\phi_{\text{EA}}(x)$ is by taking the

derivative of Eq. (13):

$$\phi_{\text{EA}}(y) = \varphi_{\text{TA}}\left(\frac{y}{1+y}\right)[(\Upsilon+1)(1+y)^\Upsilon - \Upsilon y(1+y)^{\Upsilon-1}] - \varphi'_{\text{TA}}\left(\frac{y}{y+1}\right)y(1+y)^\Upsilon. \quad (\text{B4})$$

For $\Upsilon = 0$, e.g., in the blinking-quantum-dot model, we use

$$\phi_{\text{EA}}(y) = \varphi_{\text{TA}}\left(\frac{y}{1+y}\right) - y \frac{d}{dy} \left[\varphi_{\text{TA}}\left(\frac{y}{y+1}\right) \right]. \quad (\text{B5})$$

Thus, in principle, from estimation of $\varphi_{\text{TA}}(x)$ using power spectrum, one may obtain $\phi_{\text{EA}}(x)$.

APPENDIX C: POWER SPECTRUM FOR BLINKING-QUANTUM-DOT MODEL

We substitute Eq. (41) in (16) and obtain

$$\langle S_{t_m}(\omega) \rangle / t_m = \underbrace{\int_0^1 \frac{\tilde{\omega}x \sin(\tilde{\omega}x) + \cos(\tilde{\omega}x) - 1}{\tilde{\omega}^2 x^2} dx}_I - \frac{1}{2} \underbrace{\int_0^1 \frac{\sin(\pi\alpha)}{\pi} B(x; 1-\alpha, \alpha) \frac{\tilde{\omega}x \sin(\tilde{\omega}x) + \cos(\tilde{\omega}x) - 1}{\tilde{\omega}^2 x^2} dx}_{\text{II}}. \quad (\text{C1})$$

The first term I contributes

$$I = \int_0^1 \frac{\tilde{\omega}x \sin(\tilde{\omega}x) + \cos(\tilde{\omega}x) - 1}{\tilde{\omega}^2 x^2} dx = \frac{1}{2} \text{sinc}^2\left(\frac{\tilde{\omega}}{2}\right). \quad (\text{C2})$$

For the second term II, we integrate by parts and obtain

$$\begin{aligned} \text{II} &= \frac{\sin(\pi\alpha)}{\pi} B(1; 1-\alpha, \alpha) \frac{1 - \cos(\tilde{\omega})}{\tilde{\omega}^2} - \frac{\sin(\pi\alpha)}{\pi} \frac{1}{\tilde{\omega}^2} \\ &\times \int_0^1 dx [1 - \cos(\tilde{\omega})] x^{-\alpha-1} (1-x)^{\alpha-1}. \end{aligned} \quad (\text{C3})$$

By definition, the Kummer confluent function $M(a, b; z)$ for imaginary variable is

$$\frac{\Gamma(b)}{\Gamma(a)\Gamma(b-a)} \int_0^1 du e^{i\tilde{\omega}u} u^{a-1} (1-u)^{b-a-1} \equiv M(a, b; i\tilde{\omega}). \quad (\text{C4})$$

Taking the integration over $\tilde{\omega}$ on both sides of Eq. (C4), with $a = 1 - \alpha$ and $b = 1$, gives

$$\begin{aligned} &\frac{1}{\Gamma(1-\alpha)\Gamma(\alpha)} \int_0^1 dx x^{-\alpha} (1-x)^{\alpha-1} \frac{e^{i\tilde{\omega}x} - 1}{ix} \\ &= \int_0^{\tilde{\omega}} d\tilde{\omega}_1 M(1-\alpha, 1, i\tilde{\omega}_1) = \tilde{\omega} M(1-\alpha, 2; i\tilde{\omega}), \end{aligned} \quad (\text{C5})$$

and then taking the imaginary part

$$\begin{aligned} &\frac{1}{\Gamma(1-\alpha)\Gamma(\alpha)} \int_0^1 dx x^{-\alpha-1} (1-x)^{\alpha-1} [\cos(\tilde{\omega}x) - 1] \\ &= \text{Im}[\tilde{\omega} M(1-\alpha, 2; i\tilde{\omega})]. \end{aligned} \quad (\text{C6})$$

Hence, we conclude that

$$\text{II} = \frac{1}{2} \text{sinc}^2\left(\frac{\tilde{\omega}}{2}\right) - \frac{1}{\tilde{\omega}} \text{Im}[M(1-\alpha, 2; i\tilde{\omega})]. \quad (\text{C7})$$

Evaluating $I - \text{II}/2$ in Eq. (C2) gives Eq. (42) in the main text.

APPENDIX D: SIMULATION METHODS

We use the sample power spectrum definition, i.e., $S_{t_m}(\omega) = |I_{t_m}(\omega)|^2 / t_m$. In each system, we generate the time series of the signal $I(t)$ and use discrete Fourier transform to find $I_{t_m}(\omega)$ and its complex conjugate $I_{t_m}(\omega)^*$. The simulation was done by MATLAB standard fast Fourier transform (FFT) function. At last, we average over the realizations set to find the ensemble average $\langle S_{t_m}(\omega) \rangle$. The power spectrum simulation in the renewal process may be faster by using the method below instead of using the FFT function.

1. Blinking-quantum-dot simulation

As was mentioned in the text, the process is defined with two states $I_{\text{off}} = 0$ and $I_{\text{on}} = 1$, with random sojourn times in each state $\{\tau_i\}$. The system switches states alternately, “off” \leftrightarrow “on”, every time $t_n = \sum_i \tau_i$. The random sojourn times τ_i are generated with $\tau = x^{-1/\alpha}$ where x is random uniformly distributed in the interval $(0, 1)$. With that generation process we find

$$\psi(\tau) = \alpha \tau^{-1-\alpha}, \quad \tau > 1 \quad (\text{D1})$$

i.e., $\tau_0 = 1$, and its Laplace transform is

$$\psi(s) = \alpha E_{1+\alpha}(s), \quad (\text{D2})$$

where $E_{1+\alpha}(s) \equiv \int_1^\infty t^{-1-\alpha} \exp(-st) dt$. When $s \rightarrow 0$ we find

$$\psi(s) = 1 - \Gamma(1-\alpha) s^\alpha. \quad (\text{D3})$$

The power spectrum for a single realization is defined as

$$t_m S_{t_m}(\omega) = \int_0^{t_m} I(t) \exp(-i\omega t) dt \int_0^{t_m} I(t) \exp(i\omega t) dt. \quad (\text{D4})$$

Since $I_{\text{off}} = 0$ and $I_{\text{on}} = 1$, as was mentioned above, we find

$$t_m S_{t_m}(\omega) = \sum_{\text{odds}} \int_{t_i}^{t_{i+1}} \exp(-i\omega t) dt \sum_{\text{odds}} \int_{t_j}^{t_{j+1}} \exp(i\omega t) dt. \quad (\text{D5})$$

Calculating the integrals and rearranging the equation give

$$t_m S_{t_m}(\omega) = \frac{1}{\omega^2} \sum_{i,j} e^{-i\omega(t_{i+1}-t_{j+1})} + e^{-i\omega(t_i-t_j)} - e^{-i\omega(t_i-t_{j+1})} - e^{-i\omega(t_{i+1}-t_j)}. \quad (\text{D6})$$

Using Eq. (D6) simplifies the simulations since finding the renewal times $t_i = \sum_{k=1}^i \tau_k$ is faster than finding the entire sequence of $I(t)$ and using FFT. At last, we average over the realizations set.

2. Single-file diffusion simulation details

In the single-file process we generate the signal $x(t)$ by using the method in [26]. We used the diffusion coefficient

$D = 0.5$ and the average distance between nearest particles as $a = 1$.

3. Langevin equation with logarithmic potential

We generated $x(t)$ in processes which are modeled with Eq. (64), with discretization of the Langevin equation. Namely, for single realization we use

$$x(t+dt) = x(t) - \frac{x(t)}{1+x^2(t)} dt + \eta(dt), \quad (\text{D7})$$

where the random variable $\eta(dt)$ is normally distributed with zero mean and variance $2Ddt$. Notice that we used friction coefficient $\xi = 1$ and external potential $U = \ln(1+x^2)/2$.

-
- [1] R. Kubo, M. Toda, and H. Hashitsume, *Statistical Physics II: Nonequilibrium Statistical Mechanics* (Springer, Berlin, 1995).
- [2] M. B. Priestley, *Spectral Analysis and Time Series* (Academic, London, 1981).
- [3] I. Eliazar and J. Klafter, Universal Generation of Statistical Self-Similarity: A Randomized Central Limit Theorem, *Phys. Rev. Lett.* **103**, 040602 (2009).
- [4] G. Aquino, M. Bologna, P. Grigolini, and B. J. West, Beyond the Death of Linear Response: 1/f Optimal Information Transport, *Phys. Rev. Lett.* **105**, 040601 (2010).
- [5] M. Niemann, H. Kantz, and E. Barkai, Fluctuations of 1/f Noise and the Low-Frequency Cutoff Paradox, *Phys. Rev. Lett.* **110**, 140603 (2013).
- [6] M. A. Rodríguez, Complete spectral scaling of time series: Towards a classification of 1/f noise, *Phys. Rev. E* **90**, 042122 (2014).
- [7] C. Monthus and J-P. Bouchaud, Models of traps and glass phenomenology, *J. Phys. A: Math. Gen.* **29**, 3847 (1996).
- [8] L. Silvestri, L. Fronzoni, P. Grigolini, and P. Allegrini, Event-Driven Power-Law Relaxation in Weak Turbulence, *Phys. Rev. Lett.* **102**, 014502 (2009).
- [9] J. Schrieffer, M. Clusel, D. Carpentier, and P. Degiovanni, Dephasing by a nonstationary classical intermittent noise, *Phys. Rev. B* **72**, 035328 (2005).
- [10] A. Barrat, R. Burioni, and M. Mezard, Ageing classification in glassy dynamics, *J. Phys. A: Math. Gen.* **29**, 1311 (1996); J. P. Bouchaud, L. F. Cugliandolo, J. Kurchan, and M. Mézard, in *Spin Glasses and Random Fields*, edited by A. P. Young (World Scientific, Singapore, 1998).
- [11] L. Bellon and S. Ciliberto, Experimental study of the fluctuation dissipation relation during an aging process, *Physica D (Amsterdam)* **168–169**, 325 (2002).
- [12] L. F. Cugliandolo, J. Kurchan, and G. Parisi, Off equilibrium dynamics and aging in unfrustrated systems, *J. Phys. I* **4**(11), 1641 (1994).
- [13] L. F. Cugliandolo, J. Kurchan, and L. Peliti, Energy flow, partial equilibration, and effective temperatures in systems with slow dynamics, *Phys. Rev. E* **55**, 3898 (1997).
- [14] A. Crisanti and F. Ritort, Violation of the fluctuation dissipation theorem in glassy systems: basic notions and the numerical evidence, *J. Phys. A: Math. Gen.* **36**, R181 (2003).
- [15] D. S. Dean, A. Iorio, E. Marinari, and G. Oshanin, Sample-to-sample fluctuations of power spectrum of a random motion in a periodic Sinai model, *Phys. Rev. E* **94**, 032131 (2016).
- [16] L. Cohen, Time-frequency distributions—a review, *Proc. IEEE* **77**(7), 941 (1989).
- [17] C. H. Page, Instantaneous power spectra, *J. Appl. Phys.* **23**, 103 (1952).
- [18] M. Lukovic and P. Grigolini, Power spectra for both interrupted and perennial aging processes, *J. Chem. Phys.* **129**, 184102 (2008).
- [19] P. Jung, Periodically driven stochastic systems, *Phys. Rep.* **234**, 175 (1993).
- [20] E. Bertin and J. P. Bouchaud, Dynamical ultrametricity *J. Phys. A: Math. Gen.* **35**, 3039 (2002).
- [21] J. P. Bouchaud and D. S. Dean, Aging on Parisi’s tree, *J. Phys. I (France)* **5**, 265 (1995).
- [22] G. Margolin and E. Barkai, Aging correlation functions for blinking nanocrystals, and other on-off stochastic processes, *J. Chem. Phys.* **121**, 1566 (2004).
- [23] A. Dechant, E. Lutz, D. A. Kessler, and E. Barkai, Superaging correlation function and ergodicity breaking for Brownian motion in logarithmic potentials, *Phys. Rev. E* **85**, 051124 (2012).
- [24] D. A. Kessler and E. Barkai, Infinite Covariant Density for Diffusion in Logarithmic Potentials and Optical Lattices, *Phys. Rev. Lett.* **105**, 120602 (2010).
- [25] L. Lizana, M. A. Lomholt, and T. Ambjörnsson, Single-file diffusion with non-thermal initial conditions, *Physica A (Amsterdam)* **395**, 148 (2014).
- [26] N. Leibovich and E. Barkai, Everlasting effect of initial conditions on single-file diffusion, *Phys. Rev. E* **88**, 032107 (2013).
- [27] A. Taloni, A. Chechkin, and J. Klafter, Generalized Elastic Model Yields a Fractional Langevin Description, *Phys. Rev. Lett.* **104**, 160602 (2010).
- [28] A. G. Cherstvy, A. V. Chechkin, and R. Metzler, Anomalous diffusion and ergodicity breaking in heterogeneous diffusion processes, *New J. Phys.* **15**, 083039 (2013).
- [29] F. Ionita and H. Meyer-Ortmanns, Physical Aging of Classical Oscillators, *Phys. Rev. Lett.* **112**, 094101 (2014).

- [30] A. Bodrova, A. V. Chechkin, A. G. Cherstvy, and R. Metzler, Quantifying non-ergodic dynamics of force-free granular gases, *Phys. Chem. Chem. Phys.* **17**, 21791 (2015).
- [31] E. Barkai, Aging in Subdiffusion Generated by a Deterministic Dynamical System, *Phys. Rev. Lett.* **90**, 104101 (2003).
- [32] H. Kallabis and J. Krug, Persistence of Kardar-Parisi-Zhang interfaces, *Europhys. Lett.* **45**, 20 (1999).
- [33] K. A. Takeuchi and M. Sano, Evidence for geometry-dependent universal fluctuations of the Kardar-Parisi-Zhang interfaces in liquid-crystal turbulence, *J. Stat. Phys.* **147**, 853 (2012).
- [34] N. Leibovich and E. Barkai, Aging Wiener-Khinchin Theorem, *Phys. Rev. Lett.* **115**, 080602 (2015).
- [35] A. Dechant and E. Lutz, Wiener-Khinchin Theorem for Nonstationary Scale-Invariant Processes, *Phys. Rev. Lett.* **115**, 080603 (2015).
- [36] P. Dutta and P. M. Horn, Low-frequency fluctuations in solid: $1/f$ noise, *Rev. Mod. Phys.* **53**, 497 (1981).
- [37] M. S. Keshner, $1/f$ noise, *Proc. IEEE* **70**, 212 (1982).
- [38] F. N. Hooge, T. G. M. Kleinpenning, and L. K. J. Vandamme, Experimental studies on $1/f$ noise, *Rep. Prog. Phys.* **44**, 479 (1981).
- [39] M. B. Weissman, $1/f$ noise and other slow, nonexponential kinetics in condensed matter, *Rev. Mod. Phys.* **60**, 537 (1988).
- [40] A. C. Yadav, R. Ramaswamy, and D. Dhar, Power spectrum of mass and activity fluctuations in a sandpile, *Phys. Rev. E* **85**, 061114 (2012).
- [41] M. Pelton, D. G. Grier, and P. Guyot-Sionnest, Characterizing quantum-dot blinking using noise power spectra, *Appl. Phys. Lett.* **85**, 819 (2004).
- [42] P. A. Frantsuzov, S. Volkán-Kacsó, and B. Jankó, Universality of the fluorescence intermittency in nanoscale systems: Experiment and theory, *Nano Lett.* **13**, 402 (2013).
- [43] D. Krapf, Nonergodicity in nanoscale electrodes, *Phys. Chem. Chem. Phys.* **15**, 459 (2013).
- [44] O. G. Jensen, J. P. Todoschuck, D. J. Crossley, and M. Gregotzki, Fractal linear models in geophysical models, in *Nonlinear Variability in Geophysics*, edited by D. Schertzer and S. Lovejoy, (Kluwer, Dordrecht, 1991).
- [45] B. B. Mandelbrot and J. R. Wallis, Some longrun properties of geophysical records, *Water Resour. Res.* **5**, 321 (1969).
- [46] J. Banerjee, M. K. Verma, S. Manna, and S. Ghosh, Self-organized criticality and $1/f$ noise in single-channel current of voltage-dependent anion channel, *Europhys. Lett.* **73**, 457 (2006).
- [47] B. Kaulakys and M. Alaburda, Modeling scaled processes and $1/f$ noise using nonlinear stochastic differential equations, *J. Stat. Mech.* (2009) P02051.
- [48] B. B. Mandelbrot, Some noises with $1/f$ spectrum, a bridge between direct current and white noise, *IEEE Trans. Inform. Theory* **13**, 289 (1967).
- [49] T. Graves, R. B. Gramacy, N. Watkins, and C. L. E. Franzke, A brief history of long memory, [arXiv:1406.6018v3](https://arxiv.org/abs/1406.6018v3).
- [50] G. Margolin and E. Barkai, Nonergodicity of a time series obeying Lévy statistics, *J. Stat. Phys.* **122**, 137 (2006).
- [51] S. Sadegh, E. Barkai, and D. Krapf, Five critical exponents describing $1/f$ noise for intermittent quantum dots, *New J. Phys.* **16**, 113054 (2014).
- [52] S. A. Diaz and M. Di Ventra, The role of measurement time on the universal crossover from $1/f$ to non- $1/f$ noise behavior, *J. Comput. Electron.* **14**, 203 (2015).
- [53] M. L. Boas, *Mathematical Methods in the Physical Sciences* (Wiley, Hoboken, NJ, 2006).
- [54] A. Dechant, E. Lutz, D. A. Kessler, and E. Barkai, Scaling Green-Kubo Relation and Application to Three Aging Systems, *Phys. Rev. X* **4**, 011022 (2014).
- [55] M. Abramowitz and I. A. Stegun, *Handbook of Mathematical Functions* (Dover, New York, 1972).
- [56] N. Leibovich and E. Barkai (unpublished).
- [57] K. A. Takeuchi (private communication).
- [58] F. Baumann and A. Gambassi, Ageing in the contact process: scaling behaviour and universal features, *J. Stat. Mech.* (2007) P01002.
- [59] K. A. Takeuchi, M. Kuroda, H. Chat, and M. Sano, Experimental realization of directed percolation criticality in turbulent liquid crystals, *Phys. Rev. E* **80**, 051116 (2009).
- [60] C. Godrèche and J. M. Luck, Response of non-equilibrium systems at criticality: ferromagnetic models in dimension two and above, *J. Phys. A: Math. Gen.* **33**, 9141 (2000).
- [61] J. M. Drouffe and C. Godrèche, Temporal correlations and persistence in the kinetic Ising model: the role of temperature, *Eur. Phys. J. B* **20**, 281 (2001).
- [62] P. Frantsuzov, M. Kuno, B. Janko, and R. A. Marcus, Universal emission intermittency in quantum dots, nanorods and nanowires, *Nat. Phys.* **4**, 519 (2008).
- [63] F. D. Stefani, J. P. Hoogenboom, and E. Barkai, Beyond quantum jumps: Blinking nanoscale light emitters, *Phys. Today* **62**(2), 34 (2009).
- [64] G. Margolin and E. Barkai, Nonergodicity of Blinking Nanocrystals and Other Lévy-Walk Processes, *Phys. Rev. Lett.* **94**, 080601 (2005).
- [65] M. Pelton, G. Smith, N. F. Scherer, and R. A. Marcus, Evidence for a diffusion-controlled mechanism for fluorescence blinking of colloidal quantum dots, *Proc. Natl. Acad. Sci. USA* **104**, 14249 (2007).
- [66] P. Manneville, Intermittency, self-similarity and $1/f$ spectrum in dissipative dynamical systems, *J. Phys.* **41**, 1235 (1980).
- [67] C. Godrèche and J. M. Luck, Statistics of the occupation time of renewal processes, *J. Stat. Phys.* **104**, 489 (2001).
- [68] S. B. Lowen and M. C. Teich, Fractal renewal processes generate $1/f$ noise, *Phys. Rev. E* **47**, 992 (1993).
- [69] T. E. Harris, Diffusion with “collisions” between particles, *J. Appl. Probab.* **2**(2), 323 (1965).
- [70] P. L. Krapivsky, K. Mallick, and T. Sadhu, Large Deviations in Single-File Diffusion, *Phys. Rev. Lett.* **113**, 078101 (2014).
- [71] C. Hegde, S. Sabhapandit, and A. Dhar, Universal Large Deviations for the Tagged Particle in Single-File Motion, *Phys. Rev. Lett.* **113**, 120601 (2014).
- [72] A. L. Hodgkin and R. D. Keynes, The potassium permeability of a giant nerve fibre, *J. Physiol.* **128**, 61 (1955).
- [73] R. I. Macay and R. M. Oliver, The time dependence of single file diffusion, *Biophys. J.* **7**, 545 (1967).
- [74] K. Hahn, J. Karger, and V. Kukla, Single File Diffusion Observation, *Phys. Rev. Lett.* **76**, 2762 (1996).
- [75] Q. H. Wei, C. Bechinger, and P. Leiderer, Single-File Diffusion of Colloids in One-Dimensional Channels, *Science* **287**, 625 (2000).
- [76] C. Lutz, M. Kollmann, P. Leiderer, and C. Bechinger, Diffusion of colloids in one-dimensional light channels, *J. Phys.: Condens. Matter* **16**, S4075 (2004).

- [77] S. Marksteiner, K. Ellinger, and P. Zoller, Anomalous diffusion and Lévy walks in optical lattices, *Phys. Rev. A* **53**, 3409 (1996).
- [78] H. C. Fogedby and R. Metzler, DNA Bubble Dynamics as a Quantum Coulomb Problem, *Phys. Rev. Lett.* **98**, 070601 (2007).
- [79] G. S. Manning, Limiting laws and counterion condensation in polyelectrolyte solutions I. Colligative properties, *J. Chem. Phys.* **51**, 924 (1969).
- [80] A. J. Bray, Random walks in logarithmic and power-law potentials, nonuniversal persistence, and vortex dynamics in the two-dimensional XY model, *Phys. Rev. E* **62**, 103 (2000).
- [81] A. Dechant, E. Lutz, D. A. Kessler, and E. Barkai, Fluctuations of Time Averages for Langevin Dynamics in a Binding Force Field, *Phys. Rev. Lett.* **107**, 240603 (2011).
- [82] M. Niemann, E. Barkai, and H. Kantz, Renewal theory for a system with internal states, *Math. Model. Nat. Phenom.* **11**, 191 (2016).